Atomistic Simulation of Crack Nucleation and Edge Dislocation Interaction with Tilt Grain Boundaries

Zur Erlangung des akademischen Grades eines

Doktors der Ingenieurwissenschaften

Dr.-Ing.

von der Fakultät für Maschinenbau
der Universität Karlsruhe (TH)
genehmigte

Dissertation

von

M.Sc. Yuanfeng Cheng

aus Jinxiang (VR China)

Tag der mündlichen Prüfung: 12.11.2007

Hauptreferent: Prof. Dr. rer. nat. P. Gumbsch
Korreferent: Prof. Dr. ir. E. van der Giessen

Abstract

Grain boundaries play an important role in controlling the plasticity and the mechanical strength of polycrystal metals since they can act as dislocation sinks and sources, or sites for crack nucleation. The atomistic details of the interactions between grain boundaries and other lattice defects are demanded to understand the deformation of polycrystal aggregates. This work includes atomistic simulations of the interactions between edge dislocations and [110] symmetrical tilt grain boundaries in body centred cubic tungsten using the Finnis-Sinclair interatomic potential, and between edge dislocations and $[1\bar{1}2]$ small-angle, symmetrical and asymmetrical large-angle tilt grain boundaries in face centred cubic aluminum using the embedded atom method potential. Absorption of one incoming lattice dislocation leads to rearrangements of the atomistic structure and the corresponding stress field of the grain boundaries. Dislocation pile-ups increase the stress concentration at the absorption site where dislocation transmission or reemission may occur. Results of these studies show how the impediment, transmission and reemission of dislocations are complex processes and generally depend on the sign of incoming dislocations, the interacting site at the grain boundary, the size of dislocation pile-ups, the grain boundary structure, the applied stress, and available slip systems in the neighboring grain. In tungsten, when a dislocation is absorbed by such grain boundaries, a tensile stress concentration develops below the absorption site and a crack is nucleated there under applied tensile stresses. Crack nucleation is investigated under different loading conditions. Our results show that crack nucleation is aided by both absorptions and emissions of dislocations or twins. The relevant mechanisms are significantly more complex than captured by simple pile-up models.

Kurzzusammenfassung Korngrenzen spielen eine wichtige Rolle für die Plastizität und Festigkeit von polykristallinen Metalle, da sie als Quellen und Senken von Versetzungen dienen können. Desweiteren können Risse an den Korngrenzen entstehen. Für das Verständnis der Verformung von polykristallinen Materiallien ist somit das sorgfältige Studium der Wechselwirkungen zwischen Korngrenzen und anderen Kristalldefekten notwendig. In dieser Arbeit werden mit den Methoden der atomistischen Simulation die Wechselwirkungen zwischen Stufenversetzungen und symmetrischen [110] Kipp-Korngrenzen in kubisch-raumzentriertem Wolfram sowie zwischen Stufenversetzungen und [1$\bar{1}$2] Kleinwinkel- und symmetrischen und asymmetrischen Großwinkel-Korngrenzen in flächenzentriertem Aluminium untersucht. Für die Berechnungen von Wolfram wurden Finnis-Sinclair-, für die von Aluminium EAM-(embedded atom method)-Potenziale verwendet. Absorption einer ankommenden Versetzung führt zu einer Umgruppierung der Atomstruktur sowie zu einer Änderung des Spannungsfeldes an der Korngrenze. Aufstauungen der Versetzungen erhöhen die Spannung an der Absorptionsstelle, an welcher eine Transmision oder Reemission der Versetzung erfolgen kann. Die Ergebnisse dieser Untersuchungen zeigen, dass Absorption, Transmission und Reemission von Versetzungen komplexe Prozesse darstellen, die im Detail vom Vorzeichen der ankommenden Versetzung, der Position der Wechselwirkung mit der Korngrenze, der Größe der Aufstauung am Hindernis, der genauen Korngrenz-Struktur, der extern angelegten mechanischen Spannung sowie dem vorhandenen Gleitsystem im benachbarten Korn abhängen. Im Wolfram führt die Absorption einer Versetzung an einer Korngrenze zu einer Erhöhung der Zugspannung unterhalb der Versetzung, so dass es bei einer Zugbelastung hier zu einer Rissbildung kommt. Diese Rissbildung wird im Rahmen dieser Arbeit unter verschiedenen Zugbelastungen untersucht. Es zeigt sich, dass die Rissbildung durch die Absorbtion und Emission von Versetzungen und zwillingsbildung befördet wird. Die relevanten Mechanismen sind signifikant komplexer als ihre Beschreibung in einfachen Aufstau-Modellen.

Contents

Chapter 1

Introduction

Strength of materials determines the reliability and safety of mechanical components, which is either the yield strength or fracture toughness of engineering materials responding to external forces. Yield or break of materials in service may cause disastrous losses. It is important to know the ultimate loadings that materials can endure and the mechanisms of failure. The study of material failures can be used to prevent disasters or to improve the design of material strength.

Dislocation motion carries the plastic deformation and controls the mechanism of plastic deformation in grain interiors. A dislocation is a line defect in a crystal (Fig. 1.1) and originally comes to explain the disparity in theoretical shear strength of crystal lattices and the observed. Slip bands are the early evidence of its existence. With the development of scanning electron microscopy (SEM) and transmission electron microscopy (TEM), dislocations in crystals can now be directly observed. A grain boundary (GB) is a plane defect in crystals and has geometrically five degrees of freedom. GBs can be classified as small or large-angle GBs, symmetrical or asymmetrical GBs, and tilt or twist GBs. The atomistic structures of dislocation cores and GBs can be investigated by both high resolution TEM (HRTEM) and atomistic simulations (Fig. 1.1). Previous studies show that dislocation multiplication and dislocation motion may be impeded by other dislocations and GBs, causing strain hardening; fracture of materials without pre-existing cracks often proceed by the separation of GBs involving dislocation activities near them, or void nucleation inside dislocation walls. When dislocations are absorbed at a GB, stress concentrations develop and cracks may be nucleated there under tension (Fig. 1.2). Other mechanisms of plastic deformation include mechanical twinning, GB migration, GB sliding and GB diffusion. With decreasing grain size, the strength increases following the Hall-Petch equation [1] and GBs even dominate the plastic deformation in nanocrystals [2]. The failure of materials is affected by many factors, the ambient temperature, the strain rate, the cyclic loadings leading to fatigue, the chemical environment and so on. In general, microstructure of materials, including the information of grain size, dislocation structures and GB structures, should be known to understand the failure mechanisms.

The control of the microstructure of polycrystal materials by mechanical and thermal treatment is commonly used for tailoring material properties. The modelling of the physical mechanism of GB motion has revealed, that this question has to be addressed by both a detailed geometrical description of the crystallography of GBs and a physical model to describe the local relaxation mechanism, which are beyond the purely geometrical ap-
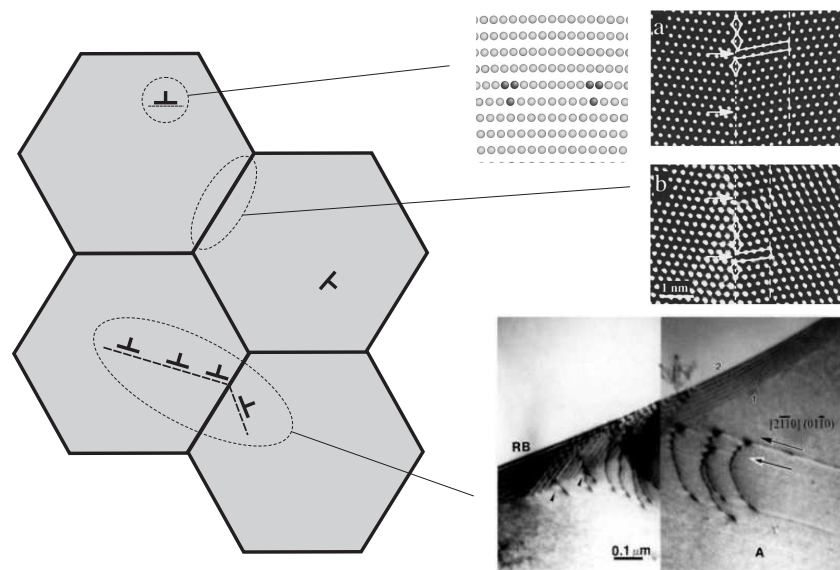
Figure 1.1: The deformation mechanisms involving dislocations and GBs in ploycrystals. Enlarged inserts (clockwise) are the dislocation core, the simulated (a) and the corresponding observed (b) atomistic structures of GBs (adapted from [3]), and the observed dislocation pile-ups at GBs (adapted from [4]).
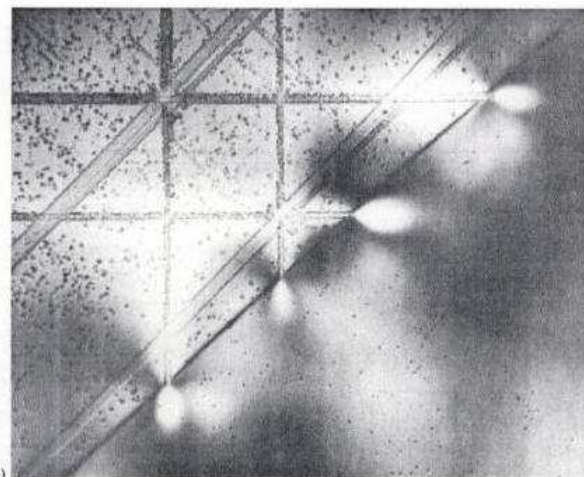

Figure 1.2: Observed stress concentrations from dislocation absorptions at a GB. Cracks can be nucleated at the absorption sites (adapted from [5]).

proach [6, 7]. In this thesis, small-angle tilt GBs in fcc aluminum and bcc tungsten with and without applied stress are studied by molecular statics. Small-angle grain boundaries (SAGBs) are distinct in mechanical, electrical (e.g. resistivity) and chemical (e.g. segregation) properties to general large-angle GBs. The successful dislocation model [8, 9, 10], where SAGBs are thought to be composed of arrays of dislocations, explains many experiments on the GB energetics and structural analysis [1]. The simple Read-Shockley model for the GB energy assumes equidistant and distinguishable edge dislocations, leading to a tilt GB. The dislocation model for GBs was originally developed for simple cubic lattices and isotropic materials, where the tilt angle between the two grains and the orientation of the GB plane are the two key parameters determining the GB energy. It predicts that the GB energy is given by $E_{GB} = E_\circ \theta (A - ln\theta)$, where θ is the misorientation angle between the two grains, $E_\circ = Gb(\cos\varphi + \sin\varphi)/4\pi(1-\nu)$ and A are functions of φ, the orientation of the GB plane with respect to the grains (ν is the Poisson's ratio) [10]. The dislocation model successfully captures the energy increase with increasing tilt angle up to $10° - 15°$. Furthermore, in a SAGB constructed by several sets of dislocations where dislocations with the same Burgers vectors in each set are parallel and evenly spaced, Frank's equation [1] (page 708) can be applied to calculate the mean spacing between dislocation cores [11, 12, 13]. Beyond this misorientation the dislocation cores overlap and the basic assumption of the model breaks down. In this case, it is better to use the fit-misfit atomic model [14] for large-angle boundaries or the Frank-Bilby equation [7](page 86) to account for the total Burgers vector content of a GB.

The transition between small and large-angle GB properties can be determined by a systematic growth and testing of bicrystals [15]. These bicrystal samples can be sheared and the motion of the SAGBs can be tracked. Furthermore the atomic structure can be observed directly for many materials. It is observed in pure metals [16, 17], superconductors [11] and natural materials (olivine) [18] that the SAGBs may be constructed by one, two or more sets of dislocations. A reconsideration of the dislocation model from simple cubic lattices to more complicated lattices (bcc, fcc, non-regular lattices, alloys *etc*) is possible by high resolution observations and atomistic simulations. For example, Bourret and Desseaux [17] pointed out three aspects not included in the dislocation model: the stability of the boundary plane, the choice of the set of Burgers vectors, which is not unique, and the effect of dislocation dissociation. In the dislocation model, different ensembles of Burgers vectors are allowed to construct geometrically the same SAGB, thus left open the question of the physical choice of a set of Burgers vectors.

The properties of SAGBs are collective behaviour of constituent dislocations and thus can be predicted by the characteristics of dislocations. Since in tilt SAGBs, the line of the constituent dislocations are along the tilt axis, it is expected that the tilt axis determines the characteristics of the constituent dislocations. From the well studied lattice dislocations with various dislocation lines, the mobility of SAGBs can be predicted based on the sessile or glissile dislocations. Furthermore, interaction between these inclined constituent dislocations is expected to limit the GB mobility. This mutual blocking mechanism is not included in the GB mobility considerations of the original dislocation model [10] but proposed by [1] (page 747). Similar to the Read-Shockley dislocation model, Penisson and Bourret [16] calculated GB energies as a function of both the tilt angle and the orientation of the GB plane and found that for the same tilt angle the GB energy was higher for

Burgers vectors inclined with the GB plane than those perpendicular to the GB plane.

To show the predictions concerning the atomic structure, the energy and the dislocation arrangement of SAGBs and their mobility under stress, molecular static simulations of selected SAGBs are performed. The investigation focuses on simple tilt GBs by varying the tilt angles, the GB planes and the tilt axes. Two materials have been chosen: (i) tungsten (bcc) as it is almost elastically isotropic and (ii) aluminum (fcc) to illuminate the effect of dislocation dissociation into GB dislocations, which is also close to isotropic. Dislocation dissociation in GB plane or perpendicular to it was observed for Diamond-cubic Ge [17], for superconductor $YBa_2Cu_3O_7$ [19] or simulated for Cu [20]. Even large-angle GBs have been shown to occasionally emit partial dislocations [21, 22]. In other cases, undissociated dislocations appear in GBs [11, 17] depending on the tilt axis. It is shown in this thesis that the simulations can provide not only the atomic structures of GBs, but also quantitative information of GB energies and mechanical properties. The investigation of the GB structures and energies show the diversity of characteristics of dislocations constructing small-angle tilt GBs. From the quantitative simulation results, the dislocation model based on the simple cubic lattices may be improved to include the characteristics of constituent GB dislocations.

Dislocation-GB interactions are studied extensively by observations, models and simulations for their importance in determining the mechanical strength of polycrystal metals [23, 24, 25, 26, 27, 28, 29, 30, 31, 32].

Observations and simulations already show that possible mechanisms of dislocation-GB interactions include dislocation absorption, transmission, reflection, and reemission at another site near the absorption site at GBs(Fig. 1.3). Dislocations can be stopped by a GB, or traverse it. A GB can also emit dislocations to grain interiors. For dislocation pile-ups at GBs, it is needed to determine which competitive slip system is activated in the neighbouring grain once the conditions are reached for dislocation transmission through GBs. Direct microscopic observations of dislocations at GBs lead to the development of criteria for the outcome of the interactions between dislocations and GBs [23, 24]. A few criteria are given to determine which slip systems are activated under dislocation pile-ups at GBs [23, 24, 33]. These criteria are closely related and consider mainly the intersection angle between the incoming and outgoing slip planes, the resolved shear stress on the outgoing slip system and the Burgers vector left at GBs after dislocation transmission.

The early transmission criterion by Livingston and Chalmers [34] determines an emitted slip system with a maximum value of $N = (e_{in} \cdot e_{out})(b_{in} \cdot b_{out}) + (e_{in} \cdot b_{out})(e_{in} \cdot b_{out})$, where e_{in} and e_{out} are the normals of the incoming and outgoing slip planes, respectively, and b_{in} and b_{out} are the Burgers vectors with subscript in and out representing the incoming and outgoing slip systems, respectively. This criterion is shown to be never satisfactory based on the experiments of Shen et al [23]. The transmission criterion given by Shen et al [23] combines two parts. The first part, called the geometric criterion, is used to determine the activated slip plane with a maximum value of $M = (I_{in} \cdot I_{out})(b_{in} \cdot b_{out})$, where I_{in} and I_{out} are the intersection lines of the incoming and outgoing slip planes with the GB, respectively. The second part is used to determine the emitted Burgers vector with a maximum Peach-Koehler force [1] in that direction provided by the pile-ups of incoming dislocations. However, as pointed out later by Lee et al [24], there is an inconsistency between the two parts of the criterion because they do not determine the sole outgoing Burgers vector,
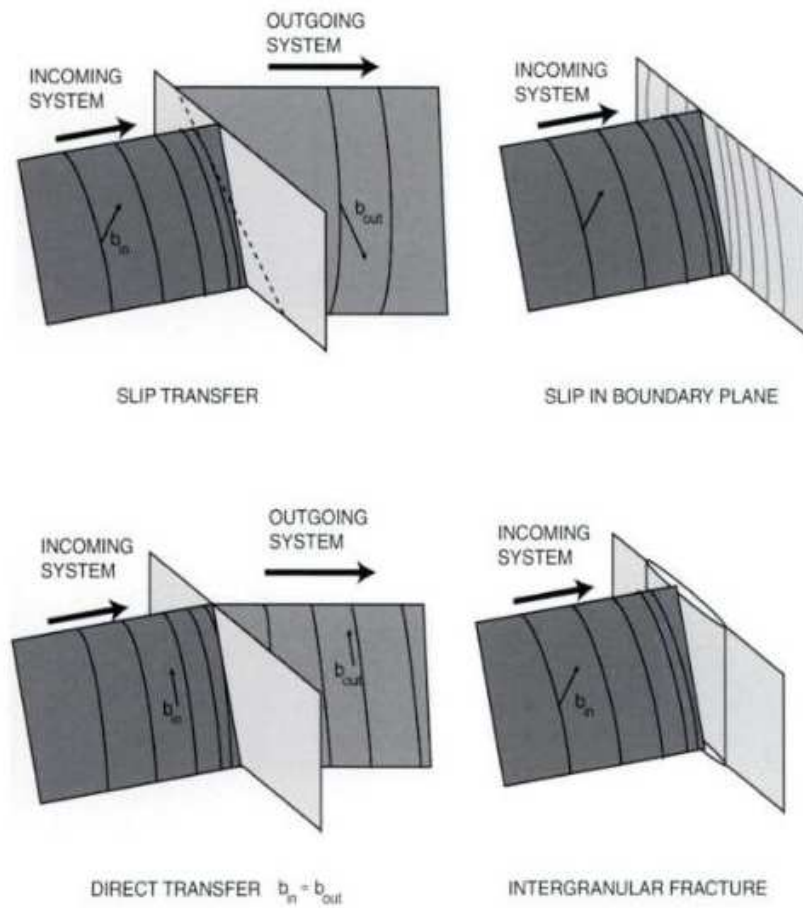
Figure 1.3: Possible mechanisms of dislocation interaction with GBs. They are dislocation absorption and reemission, dislocation absorption and propagation in GB plane, dislocation transmission and crack nucleation after dislocation absorption. (adapted from [4]).

or in other words, the Burgers vector determined by the second part may not lie in the slip plane determined by the first part of the criterion. Lee et al [24] develops a criterion combining three conditions: $I_{in} \cdot I_{out}$ should be a maximum, the residual Burgers vector at GBs after dislocation transmission should be small, and the resolved shear stress on the outgoing slip system should be high. Among the three conditions, the second condition is more stringent than the third condition, proposed by Lee et al [24]. However, there is no comparison of the quantitative contributions of these three conditions to determine the outgoing slip system. The emitted dislocations in our atomistic simulations will be discussed in chapter 7 based on the geometrical criteria.

Observations allow a first classification of possible transmission scenarios, but the detailed atomistic relaxation processes at GBs are not taken into account. Nowadays, due to the miniaturization of metallic structures in MEMS and electronic devices the plasticity and failure mechanisms at GBs are of importance. The role of GBs in the deformation of nanocrystalline materials is also investigated by many groups using atomistic simulations [2, 20, 35]. Pestman et al [29], Jin et al [36] and Zhu et al [31] studied the interaction between screw dislocations and symmetrical tilt GBs in fcc metals using atomistic simulations, both dislocation absorptions and transmissions were found depending on the structures of GBs and materials. Shenoy et al [37] and Dewald and Curtin [38] simulated the interactions between edge dislocations and symmetrical tilt GBs in fcc Al and found that dislocations were always absorbed by GBs. Koning et al [30] studied the pile-ups of dislocations generated from crack tips at three symmetrical tilt GBs in Ni and proposed a line tension model for the slip resistance of a GB to the dislocation transmission. Brandl et al [39] showed that the atomistic structure of GBs should be taken into account where they simulated a dislocation transmission only through the perfectly coherent region of a GB with mixed characteristics in Al nanocrystals. However, a systematic picture involving dislocation activities at GBs is not yet gained. From these atomistic simulations it is clear that atomistic processes are crucial for an understanding of the variety of interaction scenarios. The atomistic simulation is a complementary approach to experimental observations and analytical theories because atom rearrangement and information on stress concentrations in simulated crystalline structures help to understand the dislocation activities at GBs [20]. The analysis of nanocrystalline materials is quite complex since many different effects are superimposed such as a random network of GBs and GB dislocations, an uncontrolled stress state within the crystal due to the polycrystalline structure, which introduces elastic and plastic anisotropy. The simulations with bicrystals are much simpler in geometry and are used here. As the interactions between dislocations and GBs are atomic in scales, the investigations using bicrystals are also helpful to understand the dislocation-GB interactions in nanocrystals.

In chapter 4 the focus is on simple initially planar tilt GBs in Al and their interaction with incoming lattice dislocations. Symmetrical tilt GBs are selected to the atomistic simulations for they have repeat unit structures and the constrained freedoms of constructing GBs, therefore making the investigation much simpler. Dislocation interactions with three representative [1$\bar{1}$2] tilt GBs in Al are studied: a small-angle GB, a symmetrical Σ21 large-angle GB and an asymmetrical large-angle GB. Atomistic details of possible reactions are described, such as dislocation absorptions, transmissions and reemissions.

In chapter 5, the dislocation-GB interactions in W are shown. To study the two

factors, the GB structure itself and the angle α between incoming Burgers vectors and the normals of GBs, on the result of the dislocation-GB interactions, two kinds of distinct GB structures are selected, the coherent $\Sigma 3$ GB and two incoherent $\Sigma 9$ GBs with different α values.

Reliability and safety of components are usually assessed by means of fracture mechanics assuming preexisting cracks. In brittle materials one often assumes a statistical distribution of such initial flaws. However, decreasing structure size and increasing perfection of materials limit the applicability of this approach and make it necessary to investigate the starting point of mechanical failure, crack nucleation, in more detail. Atomistic simulations can in this case help to reveal the underlying mechanisms and conditions of crack nucleation. In the classical picture the glide of dislocations during plastic deformation is impeded by a GB and a stress concentration, which is proportional to the applied stress and the number of dislocations involved in the pile-up, develops at the obstacle [1]. When the stress at the pile-up exceeds a critical value, the material either yields by transmission of slip to the neighboring grain or a microcrack is nucleated at the boundary. The factors that determine which of these two mechanisms will occur are in general very complex and depend on intrinsic material properties as well as on extrinsic factors such as distribution of long-range internal stresses, strain rate or temperature. Clear evidence of dislocation impediment at GBs is available for a variety of materials [23, 40, 41] while experimental observations of microcrack nucleation [42] are scarce. Several suggested crack nucleation mechanisms [1] are therefore based only on indirect evidence from *post-mortem* analysis. Atomistic computer simulations can in this case provide valuable additional information about the details and conditions under which the initiation of fracture takes place. Tungsten is chosen as our model material for such simulations because it is known to be brittle at low temperatures. Polycrystal tungsten fractures predominantly by intergranular cleavage [43, 44, 45, 46]. Depending on the microstructure and loading conditions, slip and deformation twinning are competing deformation mechanisms [45]. The investigations are conducted with atomistic simulations of crack nucleation from an absorbed edge dislocation at the $\Sigma 9(2\bar{2}1)$ and the $\Sigma 9(\bar{1}14)$ [110] tilt GBs in tungsten. The aim is to develop an improved understanding of the role of GBs in strengthening metals and the role of dislocation-GB interactions for crack initiation. Since the Finnis-Sinclair potential gives an artificially weak interatomic interactions at large tensile strains, the simulations here are regarded as qualitative studies. Quantitative studies need more accurate interatomic potentials such as bond-order potentials and even ab-initio simulations, and therefore more expensive computations.

The aim of this thesis is to study systematically the atomistic-level mechanisms of the interactions between dislocation cores and GBs, and the crack nucleation at GBs. The goal is to clarify how the different structure of GBs affect dislocation motion, why and how dislocations are absorbed and transmitted, how the GB migration are affected by dislocation activities.

The thesis is organized as follows. The method of atomistic simulations with empirical potentials is introduced in chapter 2. The properties of SAGBs with and without applied stress are shown in chapter 3. The atomistic simulations of dislocation-GB interactions in fcc aluminum and bcc tungsten are presented in chapter 4 and chapter 5, respectively. In chapter 6, the simulations of crack nucleation at symmetrical tilt GBs in tungsten

are performed. The whole study is discussed in chapter 7, along with conclusions and outlooks.

Chapter 2

Simulation methods

The classical molecular dynamics simulation package IMD [47] is used in the simulations with embedded atom method (EAM) type empirical potentials to describe the interatomic interactions. The Finnis-Sinclair potential for tungsten [48, 49] and the Mishin potential for aluminum [50] are applied. The EAM potentials have the following functions [48, 50, 51]:

$$E_{pot} = \frac{1}{2} \sum_{i,j=1(j \neq i)}^{N} \phi(r_{ij}) + \sum_{i=1}^{N} U(n_i)$$

and

$$n_i = \sum_{j=1}^{N} \rho(r_{ij})$$

where ϕ is a pairwise two-body part, U is the embedding energy as a function of n, the generalized coordination of the atom, e.g. its environment, and n is a function of ρ which is a short-ranged function of pairwise interatomic distance, r_{ij}. The glue model potential, the EAM potential, the Finnis-Sinclair potential and the effective medium theory have similar analytical formulas. Since it considers the surrounding atomic structure of one atom, the EAM potential gives a better description of crystal defects like voids, dislocations and GBs than pairwise two-body potentials. However, it is still not a function of the three-body or the four-body interatomic distance and it has no term to take the interatomic angular dependence into account which is important for transition metals with covalent bonds. More advance potentials are available like bond-order potentials or even ab-initio calculations to capture more accurately atomic configurations like the core structures of dislocations, GBs and surfaces. But the computation is much more expensive than that with EAM potentials and it is still difficult to apply more advanced potentials to a simulation system with the ordinary size to EAM potentials.

Relaxation method global convergence (GLOC) [52] is applied to get the minimum energy state of the systems which mimics the $0\,K$ state. This method is a modified molecular dynamics scheme, setting velocities of all atoms to be zero, $\mathbf{v} = 0$, whenever the product of the vector of forces and the vector of velocities of all atoms is no more than zero, $\mathbf{f} \cdot \mathbf{v} \leqslant 0$, where $\mathbf{f} = (f_{1,x}, f_{1,y}, f_{1,z}, \cdots, f_{N,x}, f_{N,y}, f_{N,z})$, and $\mathbf{v} = (v_{1,x}, v_{1,y}, v_{1,z}, \cdots, v_{N,x}, v_{N,y}, v_{N,z})$.

Similar method relaxes locally singular atoms when they are passing the potential minimum [2]. More relaxation methods can be found like the conjugate gradient, adaptive GLOC and fast inertial relaxation engine (FIRE) [52, 53].

To view the atomistic structures, Gnuplot [54] and AtomEye [55] are used where atoms are shaded by the hydrostatic stress p or the common neighbor analysis (CNA) value [56]. Local atomic stress is calculated based on the virial theorem with the atomic volume calculated through the Voronoi method [2, 57, 58, 59]:

$$\sigma_{i,\alpha\beta} = \frac{1}{V_i}\Big(\frac{p_{i,\alpha}p_{i,\beta}}{m_i} - \frac{1}{2}\sum_{j\neq i}\frac{\partial E_{pot}}{\partial r_{ij}}\frac{r_{ij,\alpha}r_{ij,\beta}}{r_{ij}}\Big)$$

where $\sigma_{i,\alpha\beta}$ is the $\alpha\beta$ component of the stress tensor of atom i, V_i is the volume of atom i, p_i is its momentum and m_i is its mass. For $0\ K$, there is no contribution of temperatures to the stress calculations. So the first term in the above stress formula is not taken into account, only the internal virial (the second term) is calculated. Since $\sum_{i=1}^{N}V_i = V$, the macroscopic stress tensor of the simulation system is calculated by averaging the atomic stress over the volume V that N atoms occupy:

$$\sigma_{\alpha\beta} = \frac{1}{V}\sum_{i=1}^{N}\sigma_{i,\alpha\beta}V_i$$

Tilt GBs are created by assembling two grains with a common z axis (Fig. 2.1). Periodic boundary conditions (PBCs) are used in the y and z directions, free boundary conditions are used in the x direction. The initial distance in x between the two isolate grains is 3 Å, within the cut-off radii of the two potentials. It should be made sure that grains are not too close to overlap atoms. During relaxation, the two grains are attracted each other and the GB is constructed. The GB energy is calculated by the additional energy per area comparing to the perfect bulk system with the same number of atoms, not to take account into atoms near free surfaces. The right grain is shifted in y in $1/100$ the repeat unit length in y to find the equilibrium GB structure with the lowest energy. In W, all initial configurations are relaxed to the same structure. However, in Al, not all are relaxed to the structure with the lowest GB energy. One example is shown in Fig. 2.2 which displays two structures for geometrically the same symmetrical [110] tilt $\Sigma3(1\bar{1}2)$ GB in Al. Similar results with other EAM potentials or from ab-initio simulations for the same GB can be found in [3, 60].

PBCs are broken in the y direction by introducing dislocations in the simulation cell, but PBCs can still be used in the z direction. Several layers of outmost boundaries are created where motions of atoms are fixed in the xy plane, which are numbered from 1 to 6 in Fig. 2.3. External loadings are applied through the controlled boundary conditions. The specific usage of the six numbered boundaries is described later for different studies. The simulation box size is typically tens of nanometers in x and y and 1 nanometer in z.

Edge dislocations are created by compressing the box above the glide plane according to the corresponding Burgers vector (Fig. 2.1). The far field of the dislocation is relaxed first by fixing its core. This is followed by relaxing the core structure with free boundaries. When there are a few pile-ups of dislocations, free boundaries can not be used to avoid dislocations coming to the free surface by the image force and the repulsive force by other
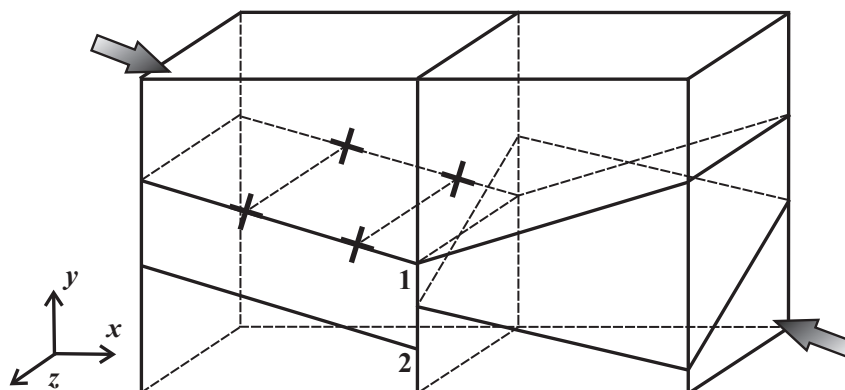
Figure 2.1: The schematic drawing of the simulated bicrystal system. A GB is located in the center of the box. Cross symbols indicate dislocations gliding on various slip planes. Arrows represent the applied loadings.
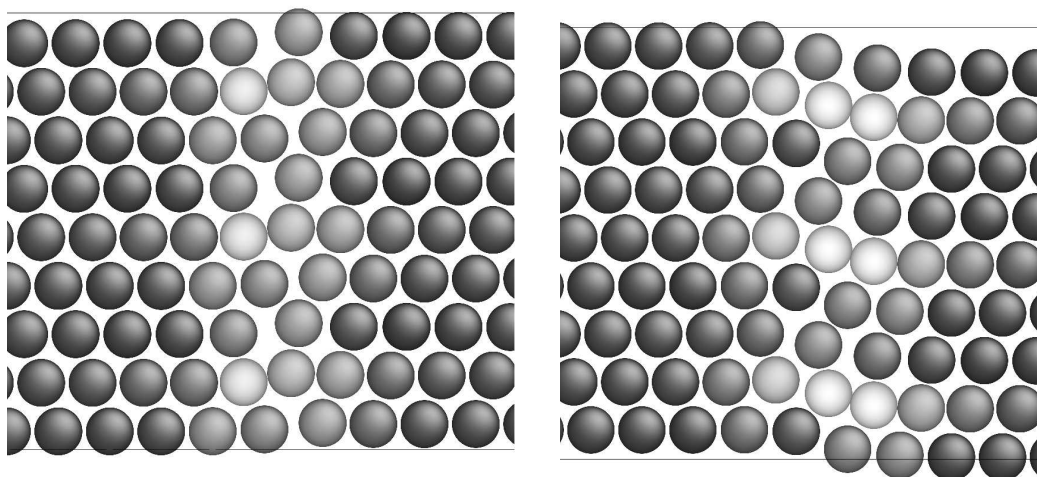

Figure 2.2: An example of searching possible GB structures with the lowest energy by shifting one grain relative to the other in y: two possible $\Sigma3(1\bar{1}2)[110]$ GB structures in Al. The GB energy of the small shift structure (left) is 0.354 J/m^2 and that of the big shift structure (right) is 0.481 J/m^2. Atoms are shaded by the hydrostatic stress. White shading means compression and black means tension.
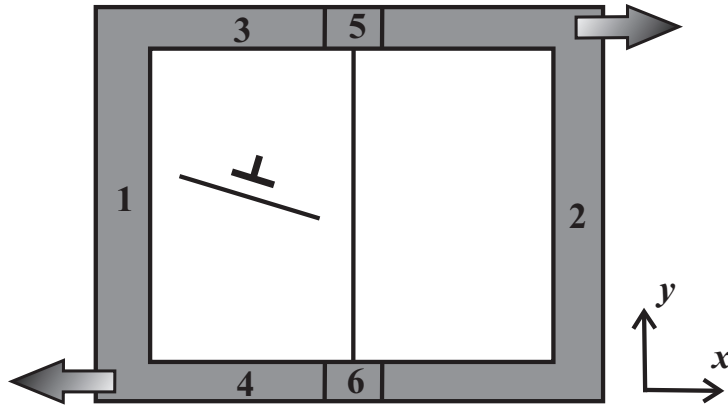
Figure 2.3: Boundary conditions of the simulation cell. Numbered outmost layers are controlled boundaries where atom motion in z is free and the motion in plane xy is controlled when external strain is applied.

dislocations. Alternatively, atom motions in x and y in boundaries numbered with 1, 2, 3 and 4 in Fig. 2.3 are fixed when relaxing dislocation cores. This can be viewed as that there is another dislocation siting at the surface which keeps others from coming closer to it. In this case, the box is in a low compressive state which is common when there are dislocation pile-ups.

In the study of small-angle GBs, to make small-angle tilt GBs, [110] tilt axis in W, [110] and [1$\bar{1}$2] tilt axis in Al are used. The setup of the bicrystals is shown in Fig. 2.4.

To study the mobility of SAGBs, simple shear strain γ_{yx} is applied by increasingly straining the system while the motions of atoms in several of the top and bottom layers (layers numbered with 3 and 4 in Fig. 2.3) are fixed in x and y, while PBCs are broken in y. Tensile strain ϵ_{xx} is applied by fixing motions in x of atoms in boundaries numbered with 1 and 2, while PBCs can still be used in y.

Dislocation interactions with the three [110] symmetrical tilt GBs in W are studied: the $\Sigma 3(\bar{1}12)$ GB, the $\Sigma 9(\bar{1}14)$ GB and the $\Sigma 9(2\bar{2}1)$ GB (Fig. 2.5). The orientations of both grains are shown in the corresponding figures in chapter 5. The size of the simulation boxes is $xyz = 400 \times 400 \times 8.95$ Å^3. An $a/2\langle 111 \rangle$ edge dislocation (a is the lattice coefficient) is introduced into one grain of a tungsten bicrystal close to the GB (20 to 40 Å), the dislocation not being attracted or repelled by the boundary during relaxation without external stresses. The dislocation line direction is along the tilt direction. Simple homogeneous shear strain γ_{yx} is then applied to the bicrystal by rigidly straining the simulation cell in steps of 0.002% or 0.05% while fixing the atom motions in boundary layers numbered with 3 and 4. The structure is relaxed after every step using the GLOC relaxation scheme [52]. The evolution of the atomistic structures and the stress field of GBs affected by the incoming dislocations are examined during the dislocation absorption and transmission.

Similar methods are used in the simulation of dislocation interactions with [1$\bar{1}$2] tilt GBs in Al in chapter 4. Dislocations with $a/2[110]$ Burgers vectors are created. The tilt axis z ([1$\bar{1}$2]) is along the direction of dislocation lines where free boundary conditions or PBCs are used, box sizes in z are 100 Å and 9.92 Å, respectively.

To study crack nucleations at GBs in W, in the first step, the $\Sigma 9(2\bar{2}1)$ tilt GB is
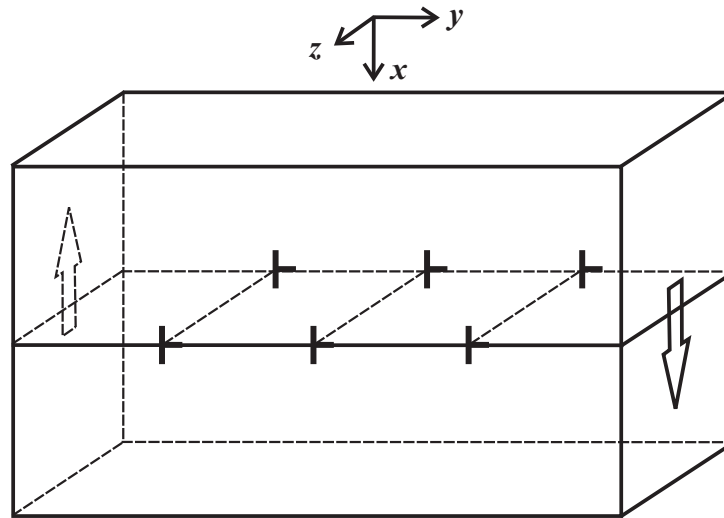
Figure 2.4: The schematic drawing of the simulated bicrystal with a small-angle tilt GB between them. Free boundary conditions are used in x and PBCs are used in z and y. PBCs in y are broken in applying shear loadings γ_{yx}. A group of dislocations with paralleled lines construct the small-angle tilt GB, the tilt axis z is along the direction of the dislocation lines.
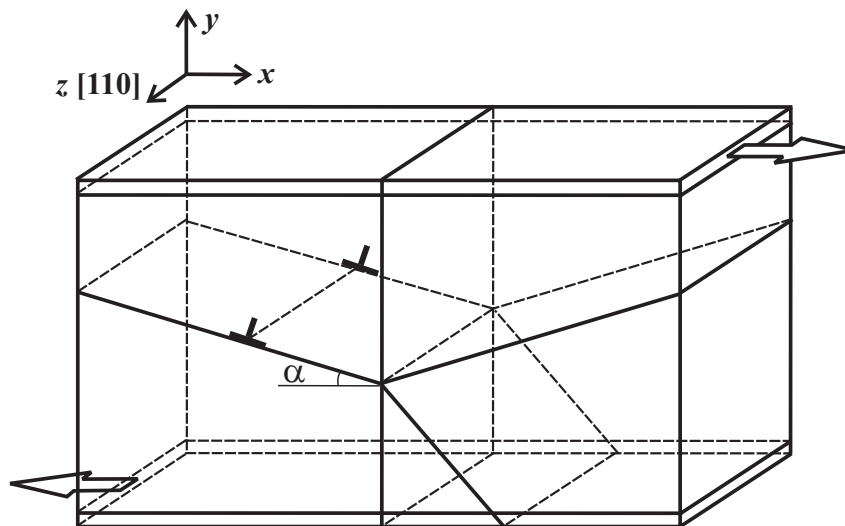

Figure 2.5: The schematic drawing of the simulation cell in the study of dislocation-GB interactions in W.

created in the center of a simulation cell. PBCs are applied in the z direction, parallel to the [110] tilt axis. Biaxial tensile strain is applied by fixing atom motions in x in boundaries numbered with 1 and 2 in Fig. 2.3 and meanwhile by fixing atom motions in y in boundaries numbered with 3 and 4. To avoid surface cracking in the study of crack nucleation at GBs, boundaries numbered with 5 and 6 in Fig. 2.3 are further created by restricting the atom motions in x. After static relaxation of the GB structure, a perfect edge dislocation with the $a/2[1\bar{1}1]$ Burgers vector is introduced in the left grain about 2 nm away from the GB, and the whole block is again fully relaxed. The dislocation line direction in this setup is parallel to the z axis of the simulation block and the dislocation core extends on the $(\bar{1}12)$ plane which is inclined by 74.21° with respect to the $(2\bar{2}1)$ GB plane. During the relaxation the position of the dislocation core does not change. It should be noted that tungsten is almost isotropic and that elastic incompatibility stresses at GBs are therefore negligible. Consequently, there are no long-range elastic forces on a dislocation near a GB. In the next step a simple shear strain is applied to the bicrystal by rigidly straining the simulation cell in steps of 0.002%. At the strain value of $\epsilon_{xy} = 0.14\%$ the dislocation starts to glide and is absorbed by the GB. In the final step of the simulation, the shear stress is removed and the block is loaded in tension either along the x axis or with a fixed ratio of $\epsilon_{yy}/\epsilon_{xx}$. The system is loaded by applying homogeneous strain in small increments, until a crack is nucleated. The analysis of the local stresses during simulation is done in terms of the usual atomic stresses. Similar method is used in the study of crack nucleation at the $\Sigma 9(\bar{1}14)$ GB. A dislocation is absorbed and twins are emitted out from the absorption site under tensile loadings and a crack follows immediately. When boundary layers 3 and 4 are freed, a twin is nucleated from the top surface and grows toward the GB. A crack is nucleated when the growing twin is stopped by the GB.

Chapter 3

Properties of small-angle tilt grain boundaries with and without applied stress

In this chapter, small-angle grain boundaries in W and Al are simulated to show the predictions in chapter 1 on the energetics and mobilities of SAGBs.

Fig. 3.1 shows the simulated GB energies of [110] tilt SAGBs in W and Al respectively, fitted to the Read-Shockley dislocation model with $A = 0.088$ for W and $A = 0.135$ for Al. Ohter constants in the dislocation model are $\varphi = 0$ for symmetrical GBs, $\nu = 0.278$, $G = 160\ GPa$, $b = a/2[111] = 2.741\ \mathring{A}$ for W, $\nu = 0.347$, $G = 28\ GPa$, $b = a/2[110] = 2.864\ \mathring{A}$ for Al, where G and b are determined by respective potentials. Both of the two series of [110] tilt SAGBs in W and Al have GB planes near $(1\bar{1}0)$. The SAGBs in W are all constructed by the same two sets of Burgers vectors, $a/2[1\bar{1}1]$ and $a/2[1\bar{1}\bar{1}]$, as the SAGB in Fig. 3.2. And the SAGBs in Al are all constructed by only one set of Burgers vectors, $a/2[1\bar{1}0]$. In good agreement with previous studies and now confirmed here that the dislocation model allows to link successfully geometrical and energetic properties of GB: SAGBs are assumed to be composed of discrete dislocations leading to the GB misorientation, and the GB energy increases with tilt angle following the increase of the GB dislocation density till dislocation cores overlap at larger misorientations. Six GBs are selected for detailed studies.

3.1 Bcc tungsten

Symmetrical and asymmetrical small-angle [110] tilt GBs are created in W with different tilt angles and GB planes. [110] tilt axis is selected to put dislocation lines and slip planes of the constituent GB dislocations in one major bcc slip systems. The constituent dislocations are therefore expected to be highly glissile.

A symmetrical SAGB with a misorientation angle of 5.40° is shown in Fig. 3.2, where the GB normal is along the [15 $\overline{15}$ 1] direction. The orientations of both grains are indicated in Fig. 3.2. The SAGB is constructed by two sets of mobile edge dislocations with Burgers vectors of $a/2[1\bar{1}1]$ and $a/2[1\bar{1}\bar{1}]$. The calculated GB energy is 1.11 J/m^2, about half that of a general large-angle GB having an energy of around 2 J/m^2. The
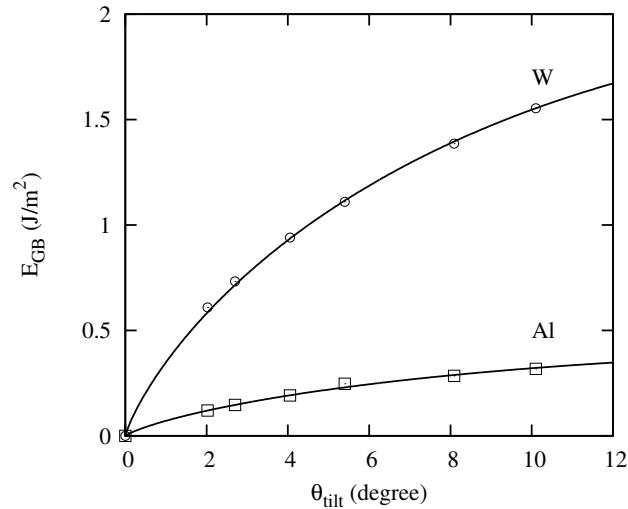
Figure 3.1: GB energy as a function of the misorietation angle for W and Al. Solid lines are from the Read-Shockley dislocation model. See text for more details.

distance in y between neighbouring dislocation cores in the simulated GB is 23.80 $\mathring{A}$, which agrees with Frank's equation (23.74 $\mathring{A}$) when taking only the component of the Burgers vectors perpendicular to the GB plane into account. Under shear loadings, the GB is found to be immobile at shear strains up to 6.0% (Fig. 3.3). The two slightly inclined dislocation types move towards each other and finally block each other.

Under tensile strain along the GB normal, a splitting of the initial SAGB is observed, as the dislocations with identical Burgers vectors in the two sets move in opposite directions (Fig. 3.4).

An asymmetrical GB is shown in Fig. 3.5. The GB plane is $(1\bar{1}\bar{1})$ and the misorientation angle is 5.77°. The calculated GB energy is 1.00 J/m^2. The Burgers vector of the only set of GB dislocations is perpendicular to the GB plane. The distance between the equally spaced dislocations is 27.20 $\mathring{A}$. Obvious GB migration is found under a simple shear strain γ_{yx} of 0.4% by the collective glide motion of the GB dislocations.

3.2   Fcc aluminum

For fcc aluminum, $[1\bar{1}2]$ tilt axis is selected to put the constituent GB dislocation lines and slip planes in one of the twelve major fcc slip systems. Therefore, the constituent dislocations are expected to be highly glissile for the $[1\bar{1}2]$ tilt axis, however, sessile for the $[110]$ tilt axis.

A symmetrical $[110]$ tilt SAGB in Al is simulated with a GB plane of $(15\ \overline{15}\ 1)$ and a tilt angle of 5.40°. Two different configurations have been found in the relaxation procedure. The lowest-energy state consists of a regular spaced GB Lomer dislocations with a distance of 30.30 $\mathring{A}$, the GB energy being 0.20 J/m^2. The other one with a higher GB energy of 0.27 J/m^2 is shown in Fig. 3.6. The GB is composed of three sets of Burgers vectors, an array of sessile $1/2[1\bar{1}0]$ dislocations embedded with 30 percent of 60° $a/2\langle 101\rangle$ dislocations which are out of plane (110) and have screw characteristics. The
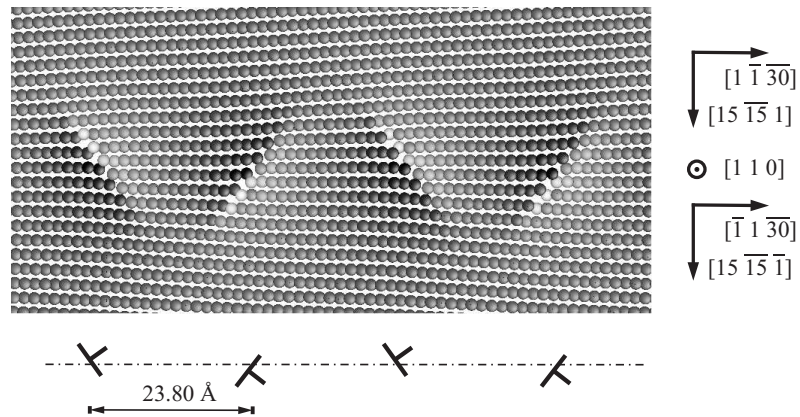
Figure 3.2: The symmetrical [110] tilt boundary in W with a GB plane of $(15\,\overline{15}\,1)$ and a tilt angle of $5.40°$. The boundary consists of two sets of $a/2\langle111\rangle$ edge dislocations which are not perpendicular to the GB plane. Atoms are shaded by the hydrostatic stress. White shading indicates compression and black indicates tension.
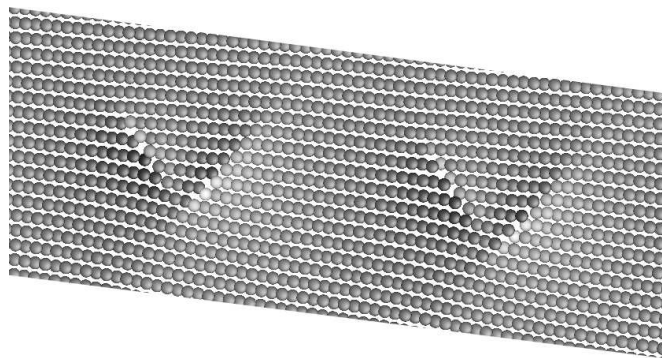

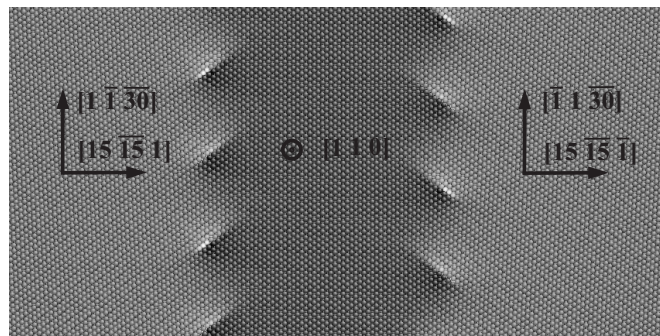Figure 3.3: Migration of the GB in Fig. 3.2 is constricted by self-block of the two sets of constituent dislocations.

Figure 3.4: The GB in Fig. 3.2 splits under tensile strain of $\epsilon_{xx} = 2.5\%$ by the opposite motion of the two sets of constituent dislocations.
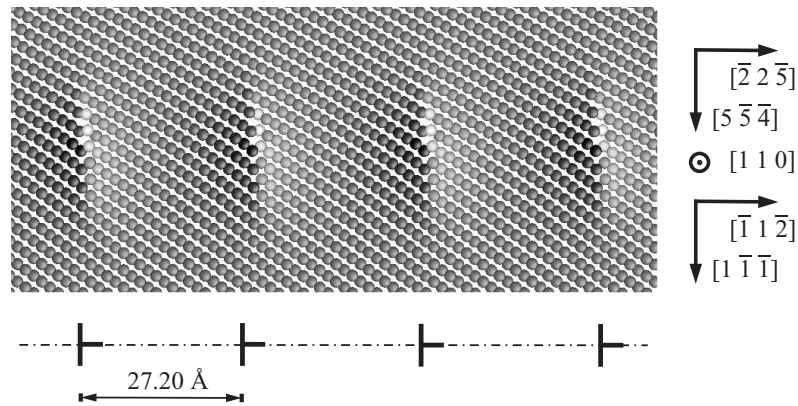
Figure 3.5: The asymmetrical [110] tilt boundary in W with a GB plane of $(1\bar{1}\bar{1})$ and a tilt angle of 5.77°. The boundary consists of only one set of edge dislocations.
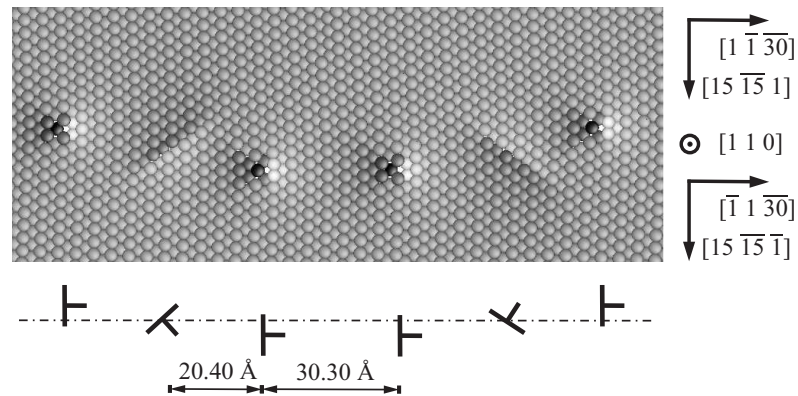

Figure 3.6: The symmetrical [110] tilt GB in Al in a high-energy state with a GB plane of $(15\ \overline{15}\ 1)$ and a tilt angle of 5.40°.

inclined dislocations are not energetically favourable and lead to faceting of the SAGB with a step height of 9.54 $\mathring{A}$. A similar GB structure with this is observed in aluminum in [16]. Both of the simulated SAGBs do not move under simple shear strains up to 5.0%, which is expected from the sessile characteristics of the constituent dislocations.

Symmetrical [1$\bar{1}$2] tilt boundaries with a GB plane of (14 16 1) and a tilt angle of 9.34° are relaxed and two different structures are found, with different GB energies. The first one, with the lower energy of 0.28 J/m^2, shown in Fig. 3.7, consists of an array of perfect dislocations, splitting into Shockley partials perpendicular to the GB plane. The width of the stacking fault is about 6.5 $\mathring{A}$ which is shorter than that of an isolated lattice dislocation with a stacking fault width of about 12.0 $\mathring{A}$. The second, in a higher-energy state, consists of isolated Shockley partials leading to a GB energy of 0.41 J/m^2 (Fig. 3.8). Both types of this GB already migrate under shear strains of 0.4% by a grouped motion of the GB dislocations.
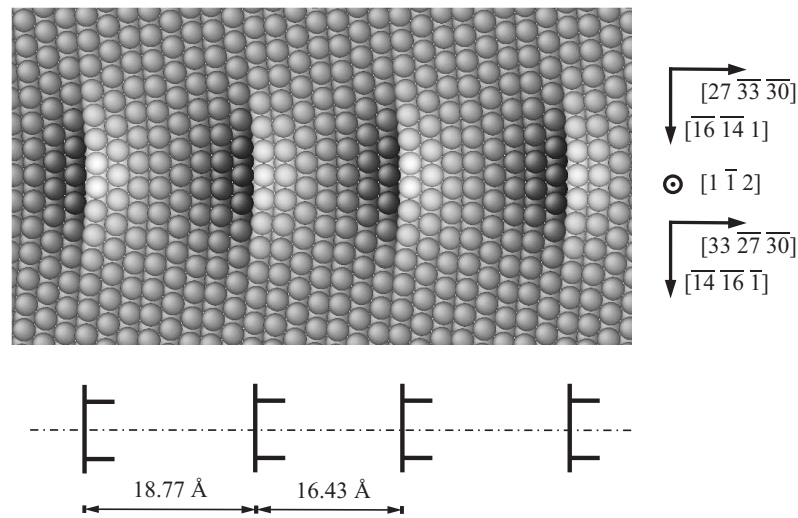
Figure 3.7: The symmetrical [1$\bar{1}$2] tilt GB in Al with a tilt angle of 9.34°, a GB plane of (110) and a GB energy of 0.28 J/m^2. There is one set of constituent Burgers vector, the perfect $a/2[110]$ dislocations which splits into Shockley partials. Dislocation cores are in a straight line with spacing each other agreeing well with Frank's equation $d = b/sin\theta = 17.60$ Å with $b = 2.86$ Å.
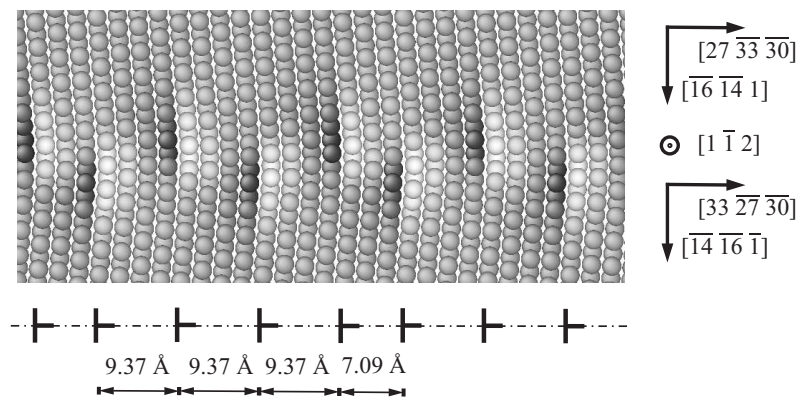

Figure 3.8: The symmetrical [1$\bar{1}$2] tilt GB in Al with the same misorientaion angle and GB plane as Fig. 3.7, with a higher GB energy of 0.41 J/m^2. There is one set of constituent Burgers vectors, the Shockley partial dislocations. Dislocation cores are wavy and the mean spacing agree well with Frank's equation $d = b/sin\theta = 8.80$ Å with $b = 1.43$ Å.

Chapter 4

Interaction between edge dislocations and tilt grain boundaries in fcc aluminum

In this chapter, the interaction between edge dislocations and three representative $[1\bar{1}2]$ tilt GBs in aluminum are simulated. A SAGB is selected because it has distinct structures to large-angle GBs and dislocation interaction with a SAGB is indeed the interaction with its constituent dislocations. Symmetrical large-angle tilt GBs are selected because they are well studied and previous counterparts can be found. An asymmetrical large-angle tilt GB is chosen for its structure is thought to be akin to random large-angle GBs, therefore to provide more general information on dislocation-GB interactions.

The $a/2[110](\bar{1}11)$ lattice edge dislocation ($a = 4.05$ Å is the lattice coefficient) is introduced into one grain of the bicrystal. The dislocation structure and its hydrostatic stress field are shown in Fig. 4.1. It shows in the figure that the dislocation splits into two Shockley partial dislocations, with the stacking fault width being 10.0 Å according to the Burgers vector plot. As shown by the atomic hydrostatic stress, there are a compressive region above the glide plane and a tensile region below, the stress level of which is comparable to that in the core of the $\Sigma21(241)[1\bar{1}2]$ symmetrical tilt GB in Fig. 4.3.

4.1 Dislocation interaction with small-angle GBs

In this section, dislocation-GB interactions are studied by pushing an edge lattice dislocation to different sites at an asymmetrical tilt SAGB.

The asymmetrical $[1\bar{1}2]$ tilt SAGB with a tilt angle $\theta = 4.67°$ and a GB energy of 0.23 J/m^2 is shown in Fig. 4.2(a). The normal of the GB plane is near [110], which is the direction of the Burgers vector $a/2[110]$ in the main slip systems of fcc materials. The SAGB is formed by an initially planar $(\bar{1}\bar{1}0)$ surface from one side and a rough surface with a normal of $[\overline{14}\ \overline{16}\ \bar{1}]$ which is close [110]. The SAGB is constructed of an array of equidistant $a/2[110](\bar{1}11)$ edge dislocations with the neighbouring distance of 35.2 Å. These glissile constituent dislocations lead to a high mobility of the SAGB. The dislocations are clearly split into Shockley partials with a step of one atomic layer between the two partials. The initial surface steps of the second grain may be the reason for this
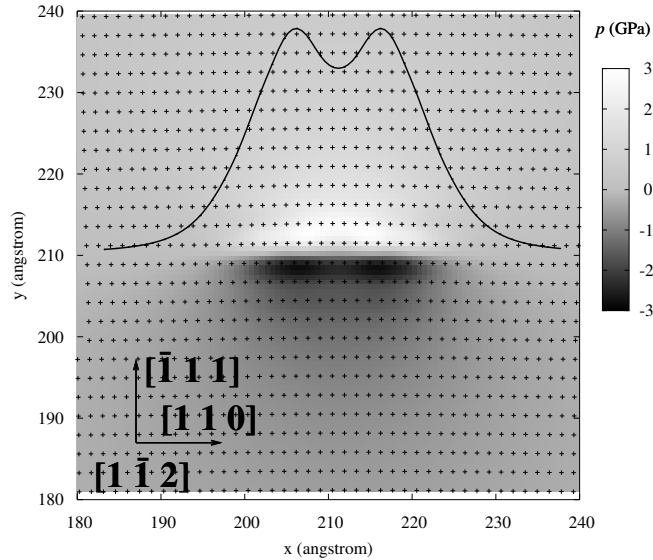
Figure 4.1: The hydrostatic stress field around the $a/2[110](\bar{1}11)$ edge dislocation core in Al. The white shading is for compression and the black for tension. The solid line is the Burgers vector plot of the dislocation core.

particular partial dislocation arrangement. Like the two realizations of geometrically the same SAGB in Fig. 3.7 and Fig. 3.8, this SAGB has another realization constructed of Shockley partial dislocations.

Two glide planes, labeled as 1 and 2 in Fig. 4.2 are chosen for the incoming lattice edge dislocations. Glide plane 1 is in plane with the GB dislocation and glide plane 2 is located in the middle of the GB structural unit. A lattice dislocation approaching on glide plane 1 annihilates with a GB dislocation if they have opposite Burgers vectors (Fig. 4.2(d)), or replace the GB dislocation by pushing it into the other grain if they the same Burgers vectors (Fig. 4.2(b)). This behaviour is expected from the elastic interactions of dislocations only. In the first case, the annihilation process, creates a row of vacancies at the location of the annihilation point of the initial GB dislocation with the incoming lattice dislocation. The vacancy row is located between the original sites of them due to the attractive elastic interaction between the incoming dislocation and the GB dislocations.

A lattice dislocation coming on glide plane 2 in figure 4.2(a) inserts into the GB (Fig. 4.2(c)) if it has the same Burgers vector as the GB dislocation, increasing the local GB misorientation accordingly. The inserted lattice dislocation (Fig.4.2(c)) does not pass through the SAGB under shear loadings but the whole GB moves by the grouped motion of the GB dislocations together with the trapped lattice dislocation. The initial SAGB can move as all GB dislocations are glissile. For opposite Burgers vector of the lattice dislocation, the SAGB acts as an obstacle to it. The lattice dislocation is attracted to the SAGB into an equilibrium position, which is found to be about 22° between the glide

plane of the lattice dislocation and the vector pointing to the closest GB dislocation from the lattice dislocation, as shown in Fig.4.2(e).

Similar results are found in the dislocation interaction with a symmetrical small-angle [1$\bar{1}$2] tilt GB with a GB plane of (14 16 1).

4.2   Dislocation interaction with symmetrical large-angle GBs

In this section, the focus is on the interaction between the $\Sigma21(241)[1\bar{1}2]$ symmetrical tilt GB and either a single or a few incoming edge dislocations.

The atomistic structure and the hydrostatic stress field of the $\Sigma21(241)[1\bar{1}2]$ symmetrical tilt GB are shown in Fig. 4.3. The orientations of both grains are indicated in Fig. 4.3. The tilt angle is 44.42°. The GB energy is 0.44 J/m^2. GB atoms are either in a high compressive or tensile stress state. The GB stress field extends only a few atom layers into the grains. Three different glide planes within the GB structural unit are marked in Fig. 4.3. Two types of situations are simulated: (i) the interaction of a single dislocation with the GB and (ii) a dislocation pile-ups against the GB. It is found that the choice of the glide plane for the incoming dislocations is crucial for the interaction result.

First, the results on single lattice dislocations are presented: the incoming dislocation on plane no. 1 and 2, starting from 80 $\mathring{A}$ away from the GB, moves towards the GB with the increasingly applied simple shear strain, γ_{yx}. As shown in figure 4.4(a-b), it is already absorbed at the current shear strain of 0.5% and a GB step is created. Comparing the absorption on plane no. 1 and 2 at the same shear strain, both partial dislocations in the perfect edge dislocation are absorbed on glide plane no. 2, whereas on glide plane no. 1 a trailing partial is left before the GB. Fig. 4.4(a) shows clearly that a trailing partial lies on one glide plane above the initial glide plane while the leading partial has been absorbed in the GB region. Since the dislocation did not meet the GB at a location where compressive and tensile stresses of the GB and the leading partial mutually annihilates, it experienced a climb force within the GB. A climb step effectively created a row of vacancy which has spread between the two partials and led to an apparent climb of the trailing partial. The total absorption of the dislocation leads to the generation of a step at the GB and a GB dislocation. The created GB dislocation moves upwards in the GB plane later under an applied shear strain of 1.5% and eventually leads to GB migration. The GB step is removed by the GB migration towards the left grain. The mechanism of the absorption of the lattice dislocation and the induced GB migration in the process of the dislocation-GB interaction is depicted in Fig. 4.5(b).

A different behaviour of dislocation-GB interactions is found for a lattice dislocation coming to the GB on glide plane no. 3. The leading partial of the lattice dislocation is not easily absorbed and stops before the GB as shown in Fig. 4.4(c1). Even if the leading partial is not yet absorbed a lateral displacement of the upper and lower part of the GB is observable. The stacking fault width between the two partials decreases to 7 $\mathring{A}$ with increasing shear, before the dislocation is absorbed at the applied shear strain of 1.125%. The absorption is accompanied by the migration of the upper part of the GB as the dislocation-GB interactions on glide plane 1 and 2. The absorption mechanism is
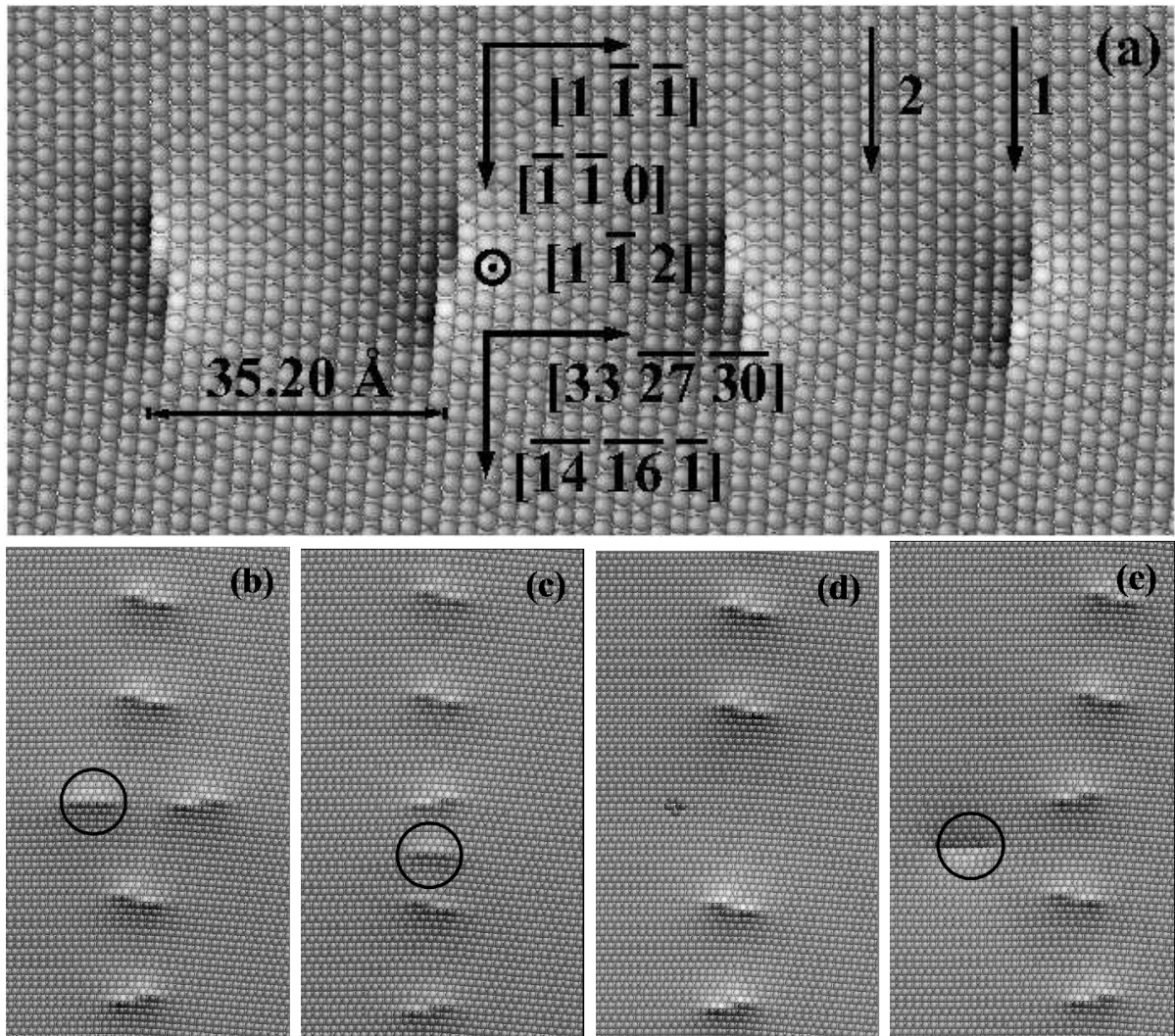
Figure 4.2: The asymmetrical $[1\bar{1}2]$ tilt SAGB in Al and the interactions with incoming lattice $a/2[110](\bar{1}11)$ edge dislocations. (a) The structure of the SAGB. (b,c) Dislocation-GB interactions with incoming lattice dislocations gliding on the plane numbered with 1 resp. 2 in (a) with the same Burgers vectors as the GB dislocations ; (d,e) Burgers vectors of lattice dislocations are inverted, respectively to (b) and (c). Loading conditions: shear load lead to an overall GB motion to the right side for (b-d) and left side for (e).
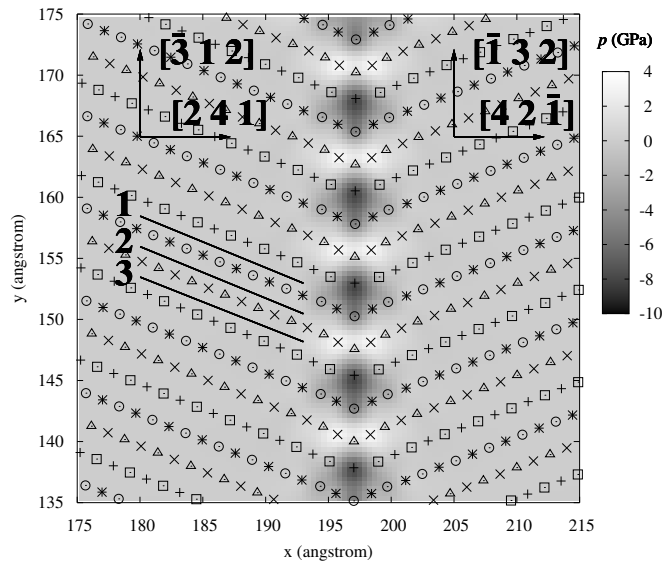
Figure 4.3: The $\Sigma21(241)[1\bar{1}2]$ symmetrical GB in Al. There are three glide planes labeled as 1, 2 and 3 ending at different stress sites in the structural unit at the GB. The six symbols present atoms on different layers in the viewing direction.

identical to the previous cases (Fig. 4.5(b)).

In all three cases, only dislocation absorption is observed. Dislocation emission from the GB could not be enforced even at applied shear strains of 5.0%. The evolution of the structure and the stress field of the GB after dislocation absorption on the three glide planes differs, which reflects different absorption processes. This is similar to the studies in tungsten which are shown in chapter 5.

Second, the influence of dislocation pile-ups on dislocation transmission/nucleation is studied for all the three lattice glide planes: in each configuration the minimum number of dislocation in the pile-up and the critical strains needed for transmission is determined. The dislocations in the pile-up include the first dislocation, which is generally incorporated in the GB as already described. It is found that two dislocations in the pile-ups coming on plane 1 and 2 are sufficient to cause dislocation transmissions. The transmission occurs as soon as the second lattice dislocation approaches the GB (Fig. 4.6(a)-(b)). The leading partial is nucleated first in the neighbouring grain and the stacking fault width reaches 15 Å before the trailing partial can escape from the GB. This is about 5 Å wider than the equilibrium spacing between the partials as shown in Fig. 4.1. The dislocation is nucleated on the mirror plane of glide plane 2 for an incoming lattice dislocation on this plane. It is not the case for lattice dislocations coming on plane no. 1. A dislocation emission occurs one layer above the mirror plane of plane 1.

Lattice dislocations on glide plane 3 lead to a different behaviour at the GB: no dislocation transmission is observed after absorption of two dislocations in the GB; the
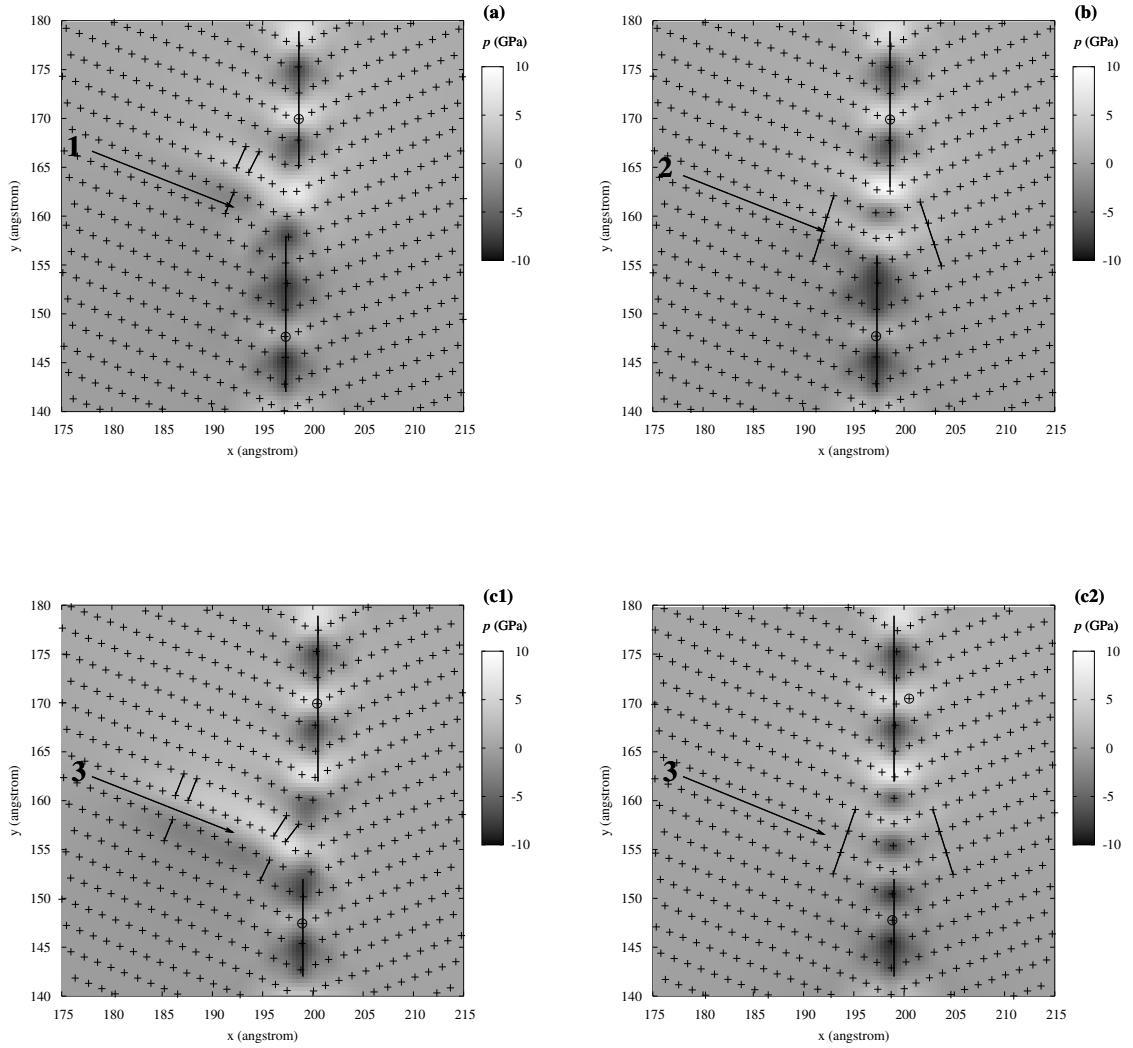
Figure 4.4: Interaction between one edge dislocation and the symmetrical $\Sigma 21(241)[1\bar{1}2]$ GB in Al. Two atoms on the original GB are marked by a circle ∘ to allow the detection of GB steps (vertical lines) and migration: (a) leading partial on plane 1 is absorbed ($\gamma = 0.5\%$); the approximate position of trailing partial is marked by three short lines; step formation is obvious; (b) Complete absorption of lattice dislocation on plane 2 ($\gamma = 0.5\%$) and step formation. (c1) The edge coming on glide plane 3 is stopped before the GB (the snapshot at $\gamma_{xy} = 0.825\%$; positions of both partials are marked) and (c2) finally absorbed at strain of 1.125% and GB migration occurred. The colors give the hydrostatic stress.
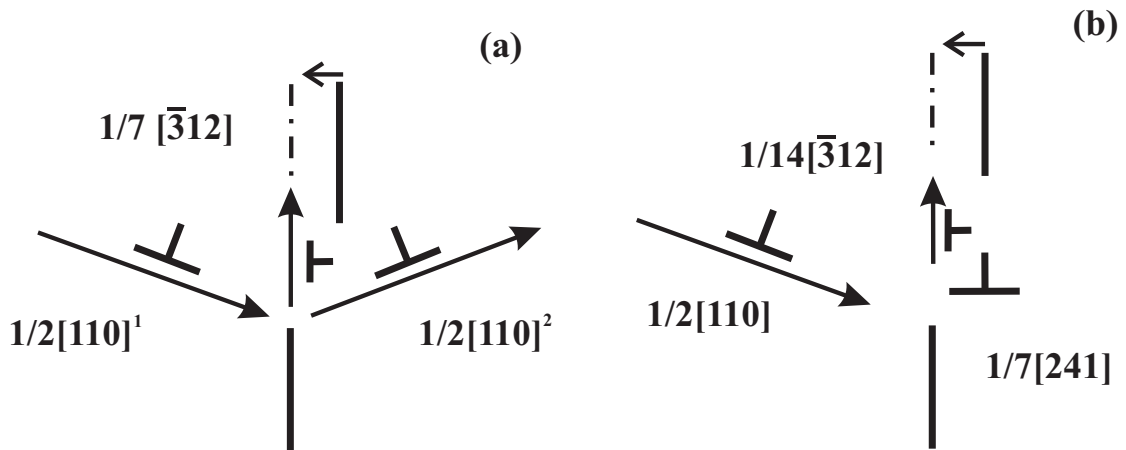
Figure 4.5: Schematic drawing of the mechanisms of the interactions between edge dislocation and the $\Sigma21(241)[1\bar{1}2]$ symmetrical GB in Al. (a) Dislocation transmission and GB migration by glide of residual GB dislocation, $a/2[110]^1 = a/7[\bar{3}12]^1 + a/2[110]^2$. (b) Dislocation absorption, $a/2[110]^1 = a/14[3\bar{1}2]^1 + a/7[241]^1$. Superscript ^{1} and ^{2} indicate respectively the left grain and the right grain.

GB becomes more disordered after absorption and atom rearrangements inside the GB occur. Thereafter the GB starts to migrate. Nucleation of a new dislocation from the GB is observed only for pile-ups containing four dislocations. In this case dislocation nucleation occurs on the glide plane one layer above the mirror plane (Fig. 4.6(c)), at the very moment when the second dislocation is going to be absorbed in the GB, which is enforced by the interaction with the remaining two dislocations in the pile-up. Similar behavior are found where two dislocations of opposite Burgers vectors with the ones here coming to the same GB on plane 3 are absorbed and no dislocation is emitted [37].

The various behaviour of dislocation-GB interactions can be explained by the stress fields of dislocations and the GB. In the interaction between the symmetrical $\Sigma21(241)[1\bar{1}2]$ GB and one incoming lattice edge dislocation on plane 1 or 2, the compressive part of the dislocation core annihilates the tensile stress field of the boundary core and vice versa, which makes dislocation absorption without stress barriers. One dislocation coming on plane 3 can be stopped before entering the GB even under an considerable shear for the compressive part of the dislocation core is repelled by the compressive stress field of the boundary core and vice versa. The mechanism of the dislocation-GB interaction involve GB migration and the creation of disconnections is shown in Fig. 4.5. It can be proposed that the mechanism is general for the interaction between edge dislocations and symmetrical tilt GBs in crystals (see also [61]). When the energy barrier of the GB migration is high because of disordered GB structures, GB migration may not occur even under sufficient shear loadings (as in Fig. 4.7).

The disconnection created at the GB resulting from dislocation absorption affects further dislocation pile-ups and different dislocation transmission behavior as shown in Fig. 4.6(a-c). For dislocation coming on plane 1, the new stress field of GB after dislocation absorption is capable of dislocation emission on the glide plane one layer above the mirror plane because the highly compressive stress is located there; For plane 2, it is exactly the mirror plane with the incoming one that is apt to emission when there are pile-ups; For

plane 3, however, it is not apt to dislocation emission for the new stress field is capable of annihilating with further coming lattice dislocation cores. When one more dislocation comes to the GB on the three glide planes where one lattice dislocation is already absorbed, the exact locations of dislocation emissions are determined in the simulation (Fig. 4.6) which are accord with the stress field analysis after absorption of the first dislocation.

When there are more (three) dislocations in the pile-up on plane 1, the critical applied shear for dislocation emission decreases from 3.0% when there are 2 dislocation pile-ups to 2.0% because more incoming dislocations generate a higher local stress concentration effectively as there are higher external loadings. According to the elastic theory of dislocation interactions, the critical applied strain for dislocation transmission is expected to be $6.0\%/n$ when the number of dislocations in the pile-up is n. Although one dislocation is already absorbed at the GB, its far-field stress field still exists and keeps the following dislocations from coming closer to the GB and stress concentration at the GB is developed for the dislocation pile-ups. However, different with the interaction between two lattice dislocations, the repulsive force between the absorbed dislocation and the further incoming dislocation is not extremely high so that the distance between them can be zero because the absorbed one is already not a perfect lattice dislocation for the atom rearrangement at the GB. In the model of dislocation pile-ups, GBs are mathematical planes. The model can be further realized by considering GBs as physical planes with finite width and atomistic properties. Regarding the physical activities of GBs in the process of interactions with dislocations, quantitative criteria of dislocation transmission for continuum studies may be proposed by measuring the distance between dislocations in atomistic simulations or by determining the strength of GBs under dislocation pile-ups.

4.3   Dislocation interaction with asymmetrical large-angle GBs

In this section, the interaction between an asymmetrical tilt GB in Al and either a single or two incoming edge dislocations is studied.

An asymmetrical large-angle $[1\bar{1}2]$ tilt GB is shown in Fig. 4.7 with a tilt angle of $74.77°$. The orientations of both grains are indicated in Fig. 4.7. The GB energy is 0.46 J/m^2, similar to the $\Sigma 21$ symmetrical tilt GB in Fig. 4.3. Different with the $\Sigma 21$ symmetrical tilt GB, there is no repeat unit structures in the asymmetrical GB. Similar to the $\Sigma 21$ symmetrical tilt GB, the width of the core of the asymmetrical tilt GB is only a few angstroms as characterized by the atomic hydrostatic stress.

A single incoming dislocation with the Burgers vector of $a/2[110]$ is absorbed at the asymmetrical GB and no dislocation emission is found up to a shear strain of 4.0%. For a pile-up containing two dislocations, the first dislocation is absorbed while the second approaches the GB with increasing shear loadings. When the second dislocation is absorbed, a mixed non-dissociated dislocation is nucleated in the neighbouring grain with the Burgers vector of $a/2[011]$ due to the periodic boundary conditions in z (Fig. 4.7).

To verify the outcome of the dislocation nucleation process, especially the dissociation of the nucleated dislocation and the choice of the activated glide plane in grain 2, a simulation without PBCs in the z direction is performed. In this case, the nucleated
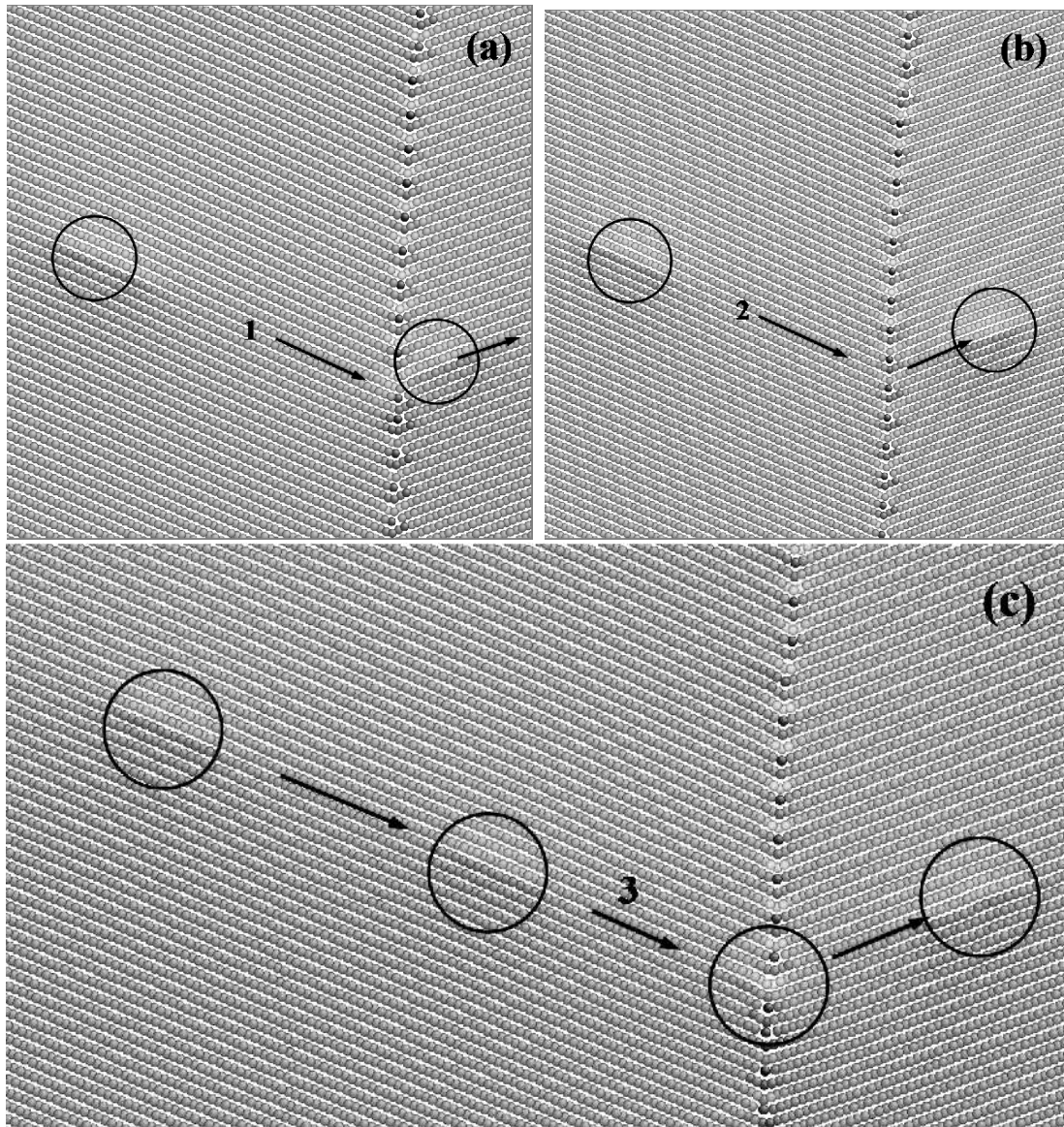
Figure 4.6: Dislocation pile-ups at the $\Sigma21(241)[1\bar{1}2]$ GB in Al and transmissions: (a) A pile-up containing two lattice dislocations coming on plane no. 1 at the GB from one grain and one dislocation transmission to the other grain on the glide plane one layer above the mirror plane of plane no. 1 ($\gamma = 3.0\%$); (b) A pile-up containing two dislocations on plane no. 2 leading to one dislocation transmission on the mirror plane of it ($\gamma = 2.2\%$); (c) A pile-up containing four dislocations coming on plane no. 3 and one dislocation transmission on a glide plane one layer above the mirror plane of it ($\gamma = 1.8\%$).
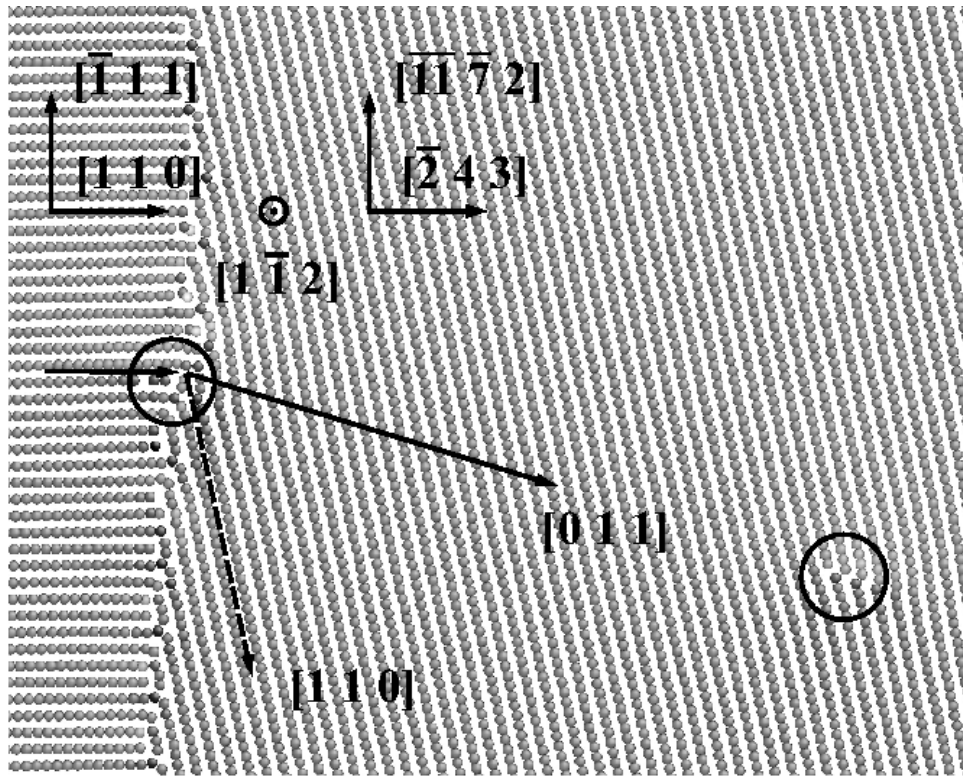
Figure 4.7: Two $a/2[110]$ edge dislocations pile-up at the asymmetrical $[1\bar{1}2]$ tilt GB in Al from the left grain and one $a/2[011]$ dislocation is emitted into the right grain($\gamma = 3.9\%$).

process is stepwise by nucleation of partial dislocations at a strain level comparable to the setup with PBCs in z, when a pile-up containing two dislocations is present, with Burgers vectors of $a/2[\bar{1}\bar{1}0]$ gliding on the plane of $(1\bar{1}\bar{1})$ as indicated by the Thompson tetrahedron in Fig. 4.8. The figure shows a time sequence of the process of dislocation absorption and nucleation: the GB structure and the nucleated dislocation currently corresponds to time t_1 just after absorption of the second dislocation in the pile-up; the structure of the second dislocation in the pile-up at time t_0 ($t_0 < t_1$) is marked with 0 in the figure. Two later stages of the emitted dislocation are marked by 2 and 3, bowing out from the GB. The nucleated dislocation has the Burgers vector of $a/2[0\bar{1}\bar{1}]$, splitting into two Shockley partial dislocations, gliding on the plane of $(11\bar{1})$. The line of the nucleated dislocation in grain 2 is not co-planar with the line of the dislocations in the pile-up in grain 1. The intersection angle between the two lines is $33.55°$.
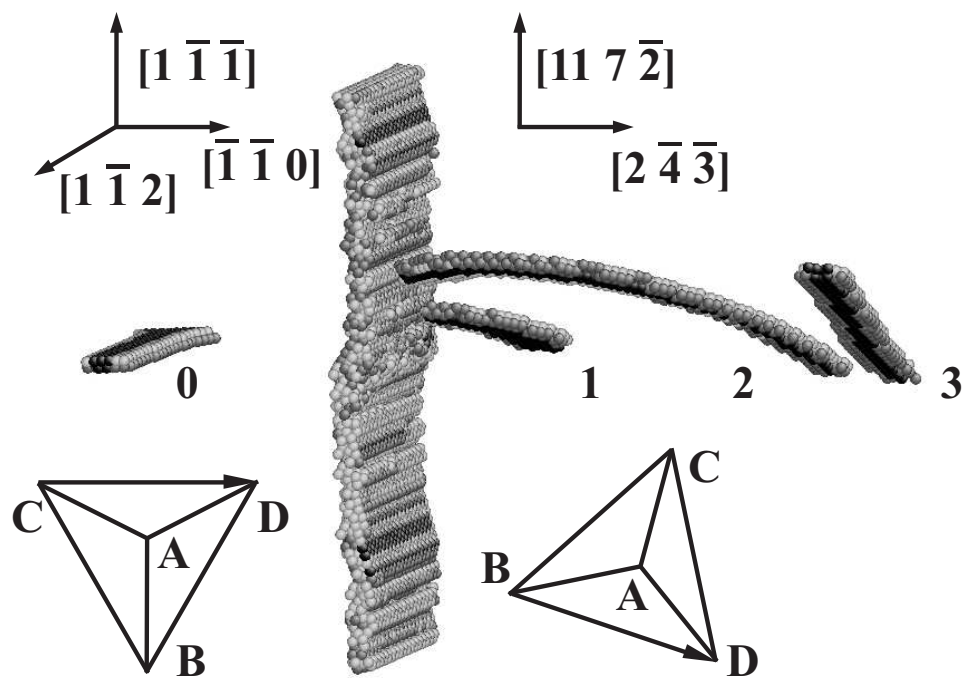
Figure 4.8: Simulation of two dislocation pile-ups at the asymmetrical [1$\bar{1}$2] tilt GB in Al from one grain and emission of one dislocation into the other grain. Atoms are shaded by the CNA values where fcc atoms are not shown. Darker atoms are in the stacking faults. After the dislocation numbered with 0 is absorbed ($\gamma = 3.6\%$), where the leading dislocation of the pile-up is already absorbed, a dislocation marked with 1 with the Burgers vector of $a/2[0\bar{1}\bar{1}]$ is nucleated later ($\gamma = 4.2\%$) from the GB. Later position of the nucleated dislocations are marked by 2 and 3.

Chapter 5

Interaction between edge dislocations and symmetrical [110] tilt grain boundaries in BCC tungsten

In this chapter, the interactions between a single $a/2\langle 111\rangle$ edge dislocation gliding on 112 planes and three symmetrical [110] tilt GBs in W are simulated. Symmetrical tilt GBs are selected for they have simple repeat unit structures, they are well studied by the CSL model, and there are previous simulations and HRTEM observations as references.

As shown by Yamaguchi and Vitek [62, 63], the core of the $1/2\langle 111\rangle$ edge dislocation lying on a $\{112\}$ plane is planar (Fig. 5.1(a)). Since the core is predominantly confined to a single plane it can be described as a continuous distribution of the Burgers vector that is shown as a solid line in Fig. 5.1(b). This distribution is asymmetrical due to the well known twinning-antitwinning asymmetry of shear on $\{112\}$ planes [64]. The smaller and higher peaks correspond to the twinning and antitwinning side of the dislocation, respectively, and may be interpreted as a dissociation into two fractional dislocations with the Burgers vectors $1/6\langle 111\rangle$ and $1/3\langle 111\rangle$.

The DGB interactions are investigated for three symmetrical [110] tilt GBs, namely, $\Sigma3(\bar{1}12)$, $\Sigma9(\bar{1}14)$, and $\Sigma9(2\bar{2}1)$. All these GBs are large-angle GBs with a high density of coincidence sites and well defined equilibrium atomic structures. The basic properties of the boundaries are summarized in Table 5.1 where θ_{tilt}, E_{gb} and $\gamma_{xy}{}^c$ are the tilt angle, the GB energy computed using the Finnis-Sinclair potential, and the critical shear strain for GB migration, respectively. With the choice of different GBs it is able to study three factors which are expected to play an important role in the process of dislocation-GB interactions: (1) the influence of the GB structure, (2) the inclination of the slip plane on which the incoming dislocation glides with the GB plane, and (3) the variation of the interaction site within the GB.
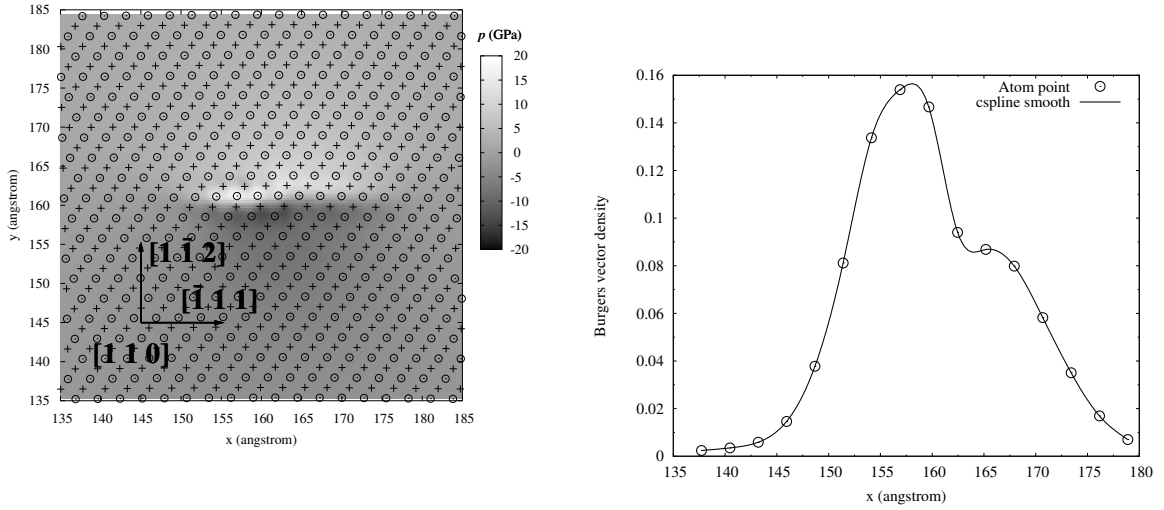
Figure 5.1: (a) The $1/2[\bar{1}11]$ edge dislocation in W lying on the $(1\bar{1}2)$ plane. (b) The corresponding plot of the Burgers vector density of the edge dislocation to show the two fractional dislocations, the bigger $1/3[\bar{1}11]$ and the smaller $1/6[\bar{1}11]$.

Table 5.1: Properties of the three boundaries

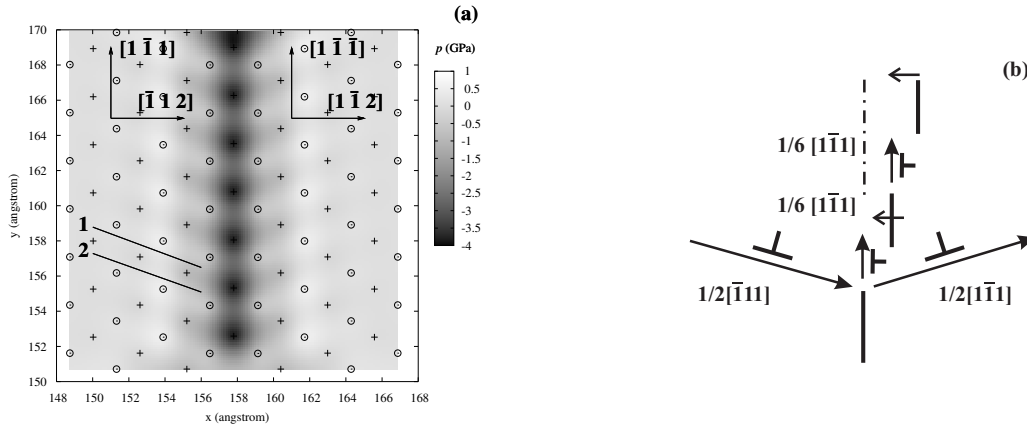| GB	θ_{tilt}	E_{gb}	α	$\gamma_{xy}{}^c$
$\Sigma3(\bar{1}12)$	$70.53°$	$0.39 J/m^2$	$19.47°$	1.6%
$\Sigma9(\bar{1}14)$	$38.94°$	$2.00 J/m^2$	$35.26°$	3.2%
$\Sigma9(2\bar{2}1)$	$38.94°$	$2.22 J/m^2$	$15.79°$	2.5%

Figure 5.2: (a) The $\Sigma3(\bar{1}12)$ coherent GB in W. White shading indicates compression, black indicates tension. Atoms are shown as circles or crosses for different height in viewing direction, [110]. (b) The schematic drawing for the transmission mechanism as in Fig. 5.3.

5.1   Dislocation interaction with the $\Sigma3(\bar{1}12)$ GB

The atomistic structure and the hydrostatic stress (p) field of the $\Sigma3(\bar{1}12)$ GB are shown in Fig. 5.2, where the orientations of both grains are indicated. The stress level of GB atoms is about 0.2 of that inside a dislocation core. This GB is coherent in structures and has the lowest GB energy among [110] tilt GBs. There are two repeatable $(1\bar{1}2)$ slip planes ending at different sites at the GB, labeled as 1 and 2 in Fig. 5.2(a). An edge dislocation coming from either plane can traverse through the GB under applied simple shear strains of 0.5%. Snapshots of the local atom motion and the evolution of the stress field of the GB during dislocation traversing are shown in Fig. 5.3. The transmission mechanism is drawn schematically in Fig. 5.2(b), including the creation of two $a/6[1\bar{1}1]$ GB dislocations and the migration of the upper part of the GB. As the edge dislocation approaches the GB, the leading fractional dislocation, $1/6[\bar{1}11]$, incorporates into the GB first. When the trailing fractional dislocation, $1/3[\bar{1}11]$, enters the GB and a fresh $1/3[1\bar{1}1]$ fractional dislocation is immediately emitted in the right grain, the first $a/6[1\bar{1}1]$ GB dislocation is created and moves upwards away from the absorption site. The traversed $1/3[1\bar{1}1]$ fractional lattice dislocation stays in the next grain and does not leave the GB immediately. When the transmitted dislocation leaves the GB under a higher strain of 1.2%, the other $1/6[1\bar{1}1]$ fractional trailing dislocation is nucleated and the second GB dislocation is created. The two created GB dislocations move upward in the GB plane and cause the GB migration, which restores the original GB structure and makes effectively twin growth.

5.2   Dislocation interaction with the $\Sigma9(\bar{1}14)$ GB

The structure and the hydrostatic stress field of the $\Sigma9(\bar{1}14)$ GB are shown in Fig. 5.4(a). Unlike in the coherent $\Sigma3$ boundary, the stress level of GB atoms here is of the same order
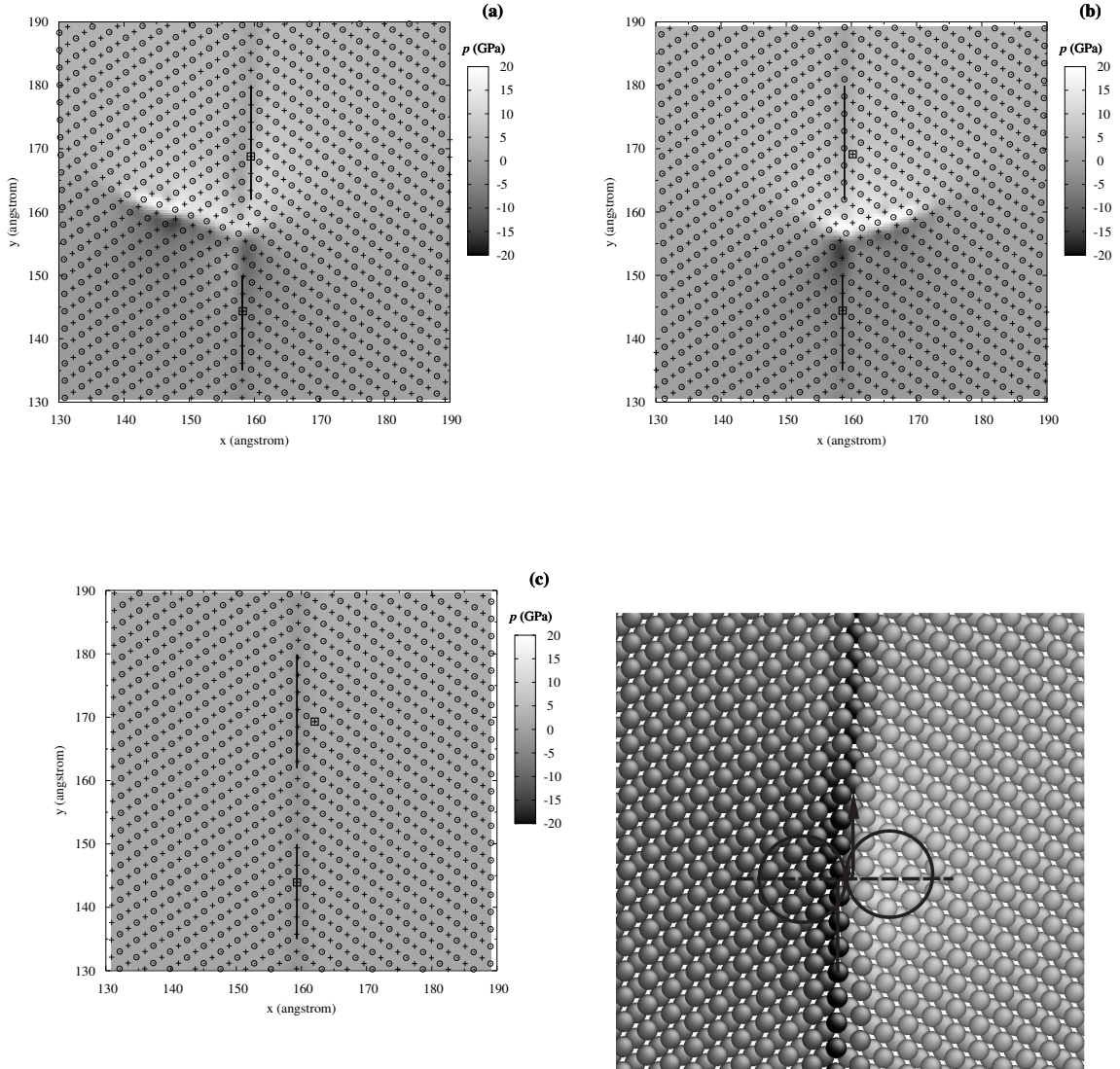
Figure 5.3: Snapshots of the dislocation traversing the $\Sigma3(\bar{1}12)$ GB in W. (a)Dislocation motion is stopped by the GB (current applied simple shear strain $\gamma_{xy} = 0.1\%$). (b) The lattice dislocation is transversing the GB ($\gamma_{xy} = 0.5\%$). (c) After transmission the original GB structure is restored by the migration of the upper part of the GB to left by two atomic layers ($\gamma_{xy} = 1.2\%$). (d) The upward propagation of the GB dislocation created during dislocation transmission. Two atoms are traced by marks of $\boxdot$, which are situated on the original GB plane. GB positions are marked by vertical lines. The relative position of the marked atoms and the current boundary plane shows the GB step and the migration of the GB. Notice also the motion of GB dislocations in (a-c), as depicted in Fig. 5.2(b).
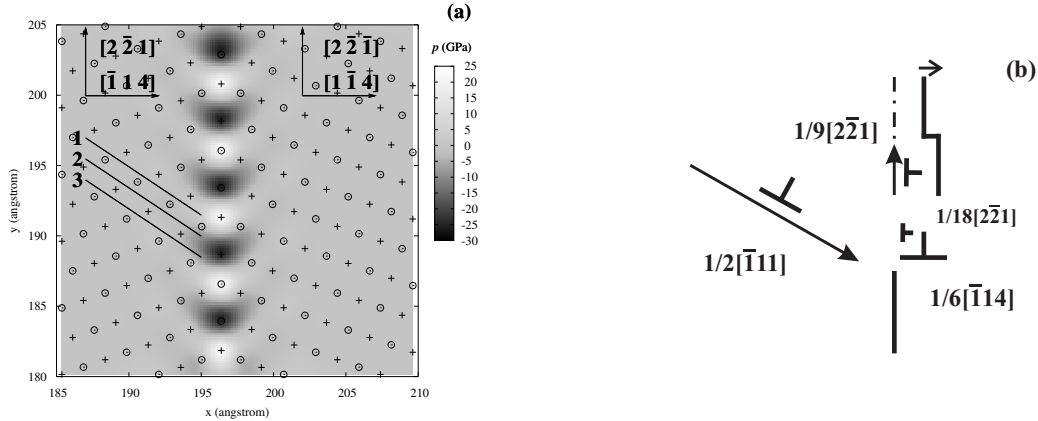
Figure 5.4: (a) The $\Sigma 9(\bar{1}14)$ GB in W. (b) The schematic drawing of the mechanism of dislocation absorption as in Fig. 5.5.

as that of a dislocation core. The width of the core of the GB is only a few angstroms as characterized by the hydrostatic stress field. There are three slip planes ending at different sites at the boundary as labeled as 1, 2 and 3 in Fig. 5.4(a). A dislocation coming from the left grain on plane 1 is stopped by the GB when the applied strain is small (0.3%). The compressive part of the dislocation core impacts to the compressive atoms in the GB, thus the repulsion stops the dislocation (Fig. 5.5(a1)). Though there is a repulsive force to the coming dislocation on glide plane 1, it is absorbed under higher strains of 0.9% by atom rearrangements in the GB plane (Fig. 5.5(a2)). Fig. 5.6 shows the change of the far stress field of the dislocation before and after entering the GB. A rotation of the Burgers vectors from the lattice dislocation to the GB dislocation is clearly captured. When a dislocation core comes from plane 2 or 3, its compressive part impacts the atoms in the GB at a location where the GB atoms are in a tensile stress state. The oppositely stressed regions lead to an attraction and locally to a mutual annihilate of the stress fields of the dislocation and the GB, therefore the dislocation is absorbed. The absorption creates a GB step plus a GB dislocation shown in Fig. 5.5, which is schematically shown in Fig. 5.4(b). Two thirds of the created GB dislocation moves upwards in the GB plane under the applied shear strain of 0.9%. Its motion leads to the migration of the upper part of the GB to the right grain, which in this case increases the GB step. The critical shear strain (0.9%) here for the migration of the GB caused by the motion of the created GB dislocation is much less than the migration of the pure GB (3.2%, in Table 5.1).

5.3   Dislocation interaction with the $\Sigma 9(2\bar{2}1)$ GB

The structure of the $\Sigma 9(2\bar{2}1)$ GB and the hydrostatic stress field are shown in Fig. 5.7. A region of high stresses is clearly visible in the immediate vicinity of the GB extending only a few atomic layers to either sides.

An edge dislocation approaching the GB on glide plane 1 among the five repeatable
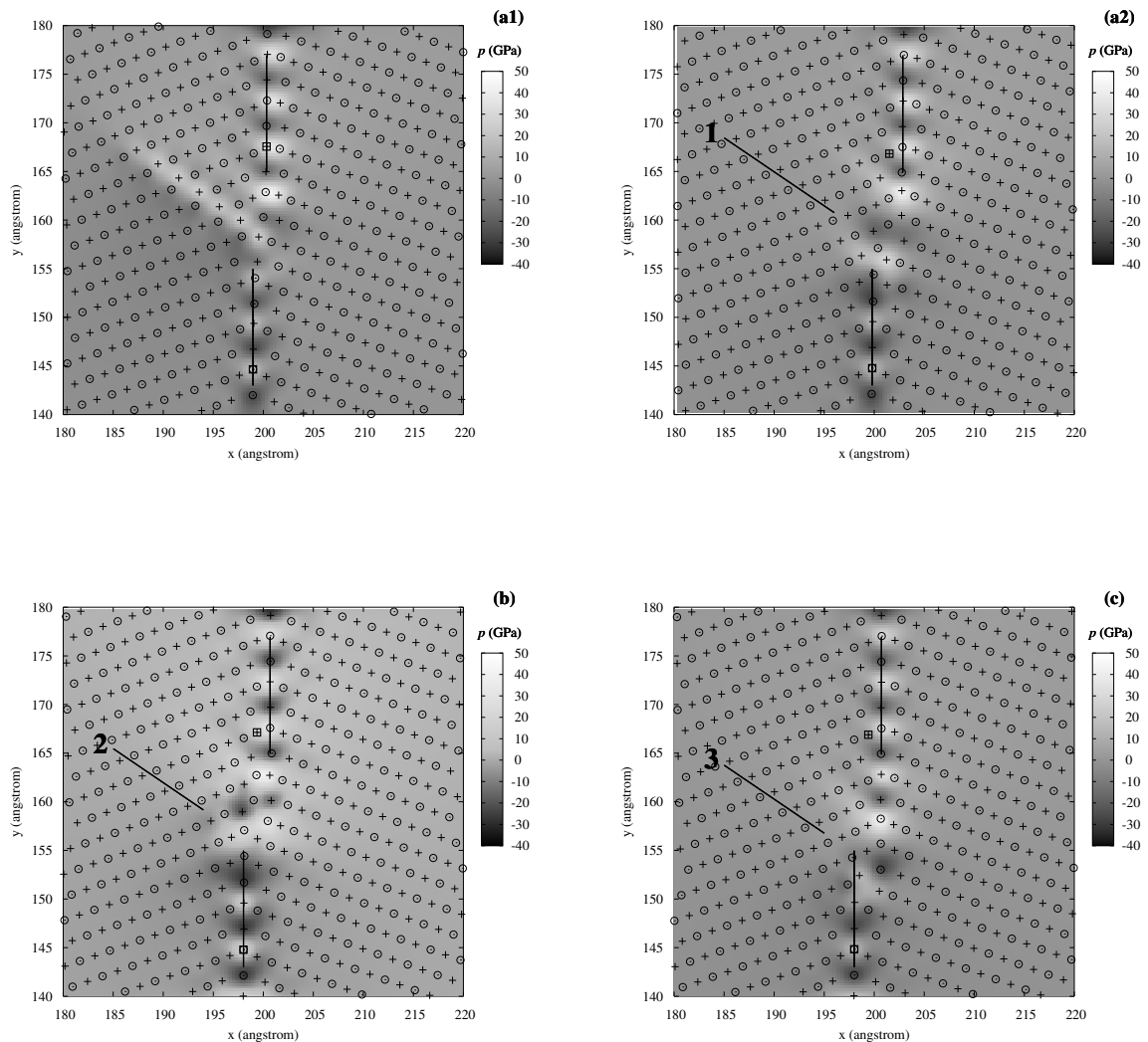
Figure 5.5: Dislocation absorption at the $\Sigma 9(\bar{1}14)$ GB in W coming on all the 3 planes depicted in Fig. 5.4(a). (a1) Dislocation coming on plane 1 is stopped before entering the GB. The current simple shear strain is 0.3%. (a2) The lattice dislocation coming on plane 1 is absorbed as the shear strain is increased to 0.9%. (b) The lattice dislocation is absorbed coming on plane 2 and (c) plane 3.
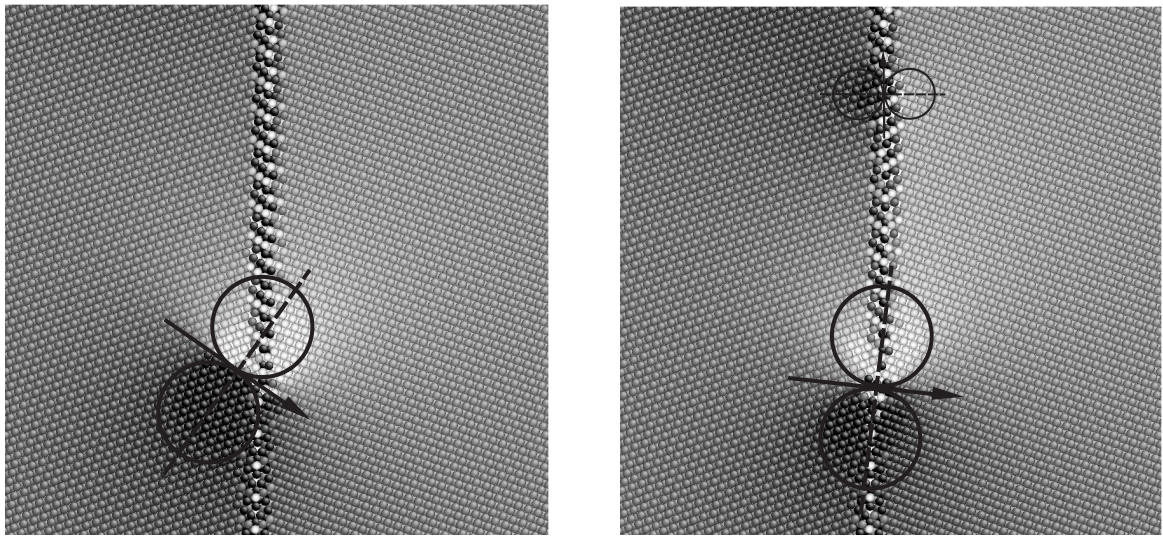
Figure 5.6: The stress field before (left) and after (right) the lattice dislocation entering the $\Sigma9(\bar{1}14)$GB in W on plane 1, corresponding respectively to Fig. 5.5(a1) and (a2).

glide planes as indicated in Fig. 5.7 arrives at the location in the boundary where the stress field of the boundary has the same sign as the stress field of the dislocation itself. Consequently, the dislocation is repelled by the boundary and stopped about 10 $\mathring{A}$ before reaching the boundary as in Fig. 5.8(a1). When the applied strain is increased to 1.4%, the dislocation traverses the boundary. The transmission is accompanied by the migration of the lower part of the GB (Fig. 5.8(a2)). The distance of the dislocation relative to the GB in x is shown in Fig. 5.9 as the applied shear strain is being increased. It shows that the distance changes not gradually, but abruptly with the applied shear strain.

In contrast, a dislocation approaching the GB on any other plane (2 to 5) leads to local atom rearrangements in the boundary plane. The dislocation is not able to leave the boundary again under the applied strain of 2.0%. A superimposed tensile stress normal to the GB plane can cause crack nucleation below the site of the absorbed dislocation (chapter 6).
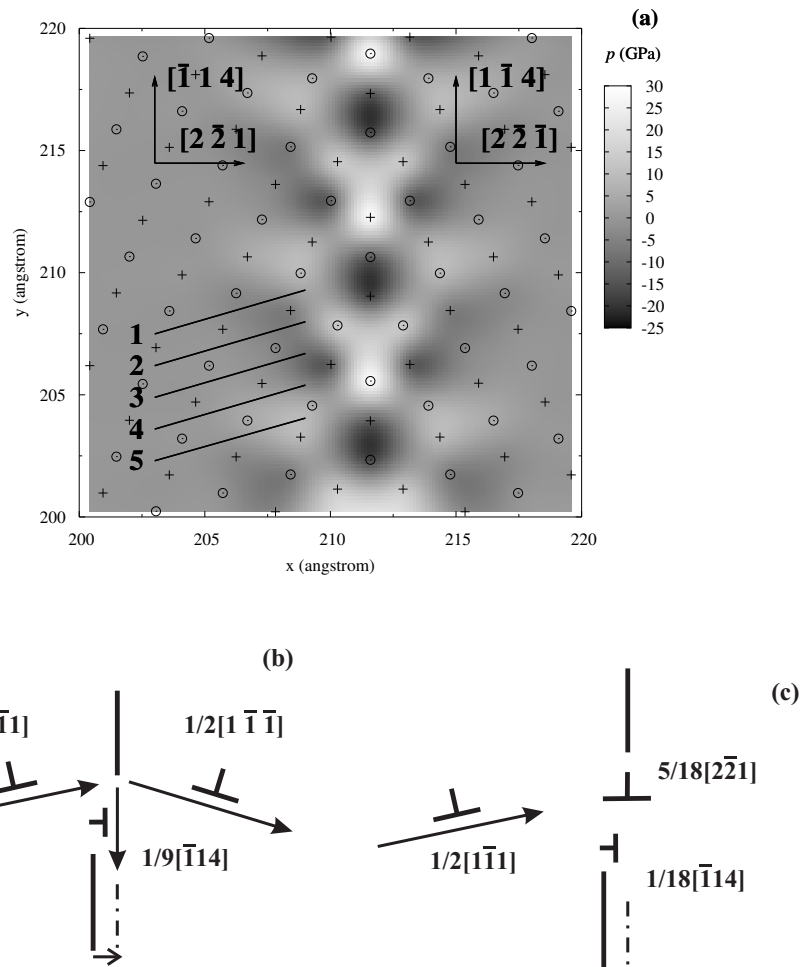
Figure 5.7: (a) The structure and the hydrostatic stress field of the $\Sigma 9(2\bar{2}1)$ GB in W. Also indicated are five repeatable $(\bar{1}12)$ glide planes ending within one structural unit. (b) The schematic drawing of the mechanism of the dislocation transmission through the GB and (c) absorption, as shown in Fig. 5.8.
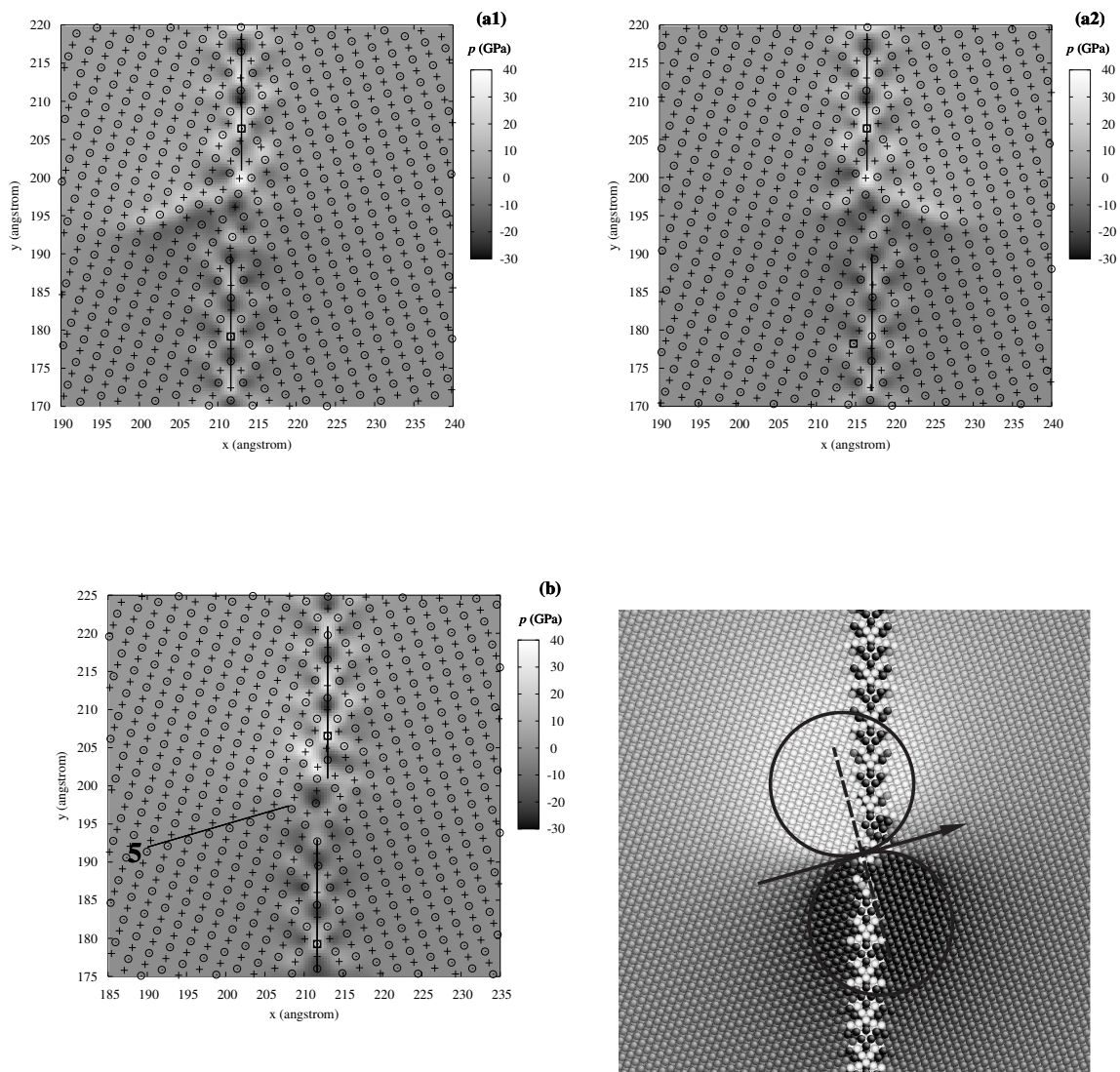
Figure 5.8: (a1) The motion of an edge dislocation coming on plane 1 is stopped by the $\Sigma9(2\bar{2}1)$ GB in W ($\gamma_{xy} = 0.4\%$). (a2) It traverses through the boundary ($\gamma_{xy} = 1.6\%$) on glide plane 1. (b) An lattice edge dislocation coming on glide plane 5 is absorbed into the GB ($\gamma_{xy} = 0.2\%$). (c) The corresponding far stress field to (b) after dislocation absorption at the $\Sigma9(2\bar{2}1)$ GB. Atoms are shaded by the hydrostatic stress.
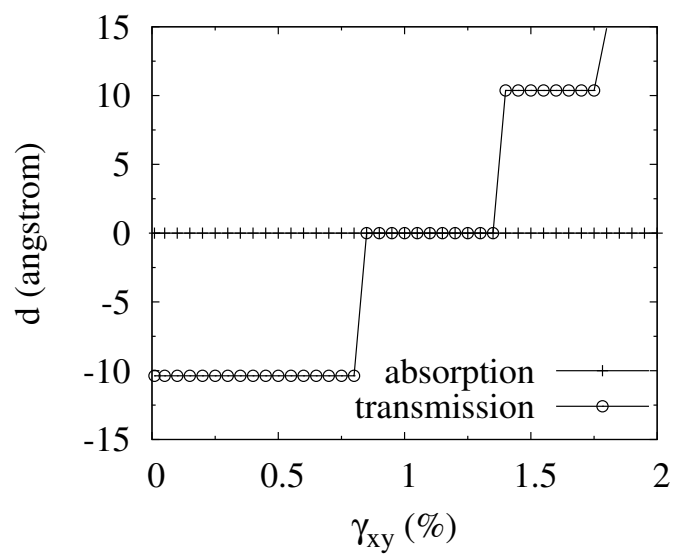
Figure 5.9: Location of the dislocation d with respect to the $\Sigma 9(2\bar{2}1)$ GB plane in x as a function of the applied shear strain.

Chapter 6

Crack nucleation in W

In this chapter, crack nucleations involving absorption/emission of dislocations/twins at two symmetrical [110] tilt GBs in W are simulated. The structures, energies, stress fields and interactions with incoming dislocations of two GBs, the $\Sigma9(2\bar{2}1)$ GB and the $\Sigma9(\bar{1}14)$ GB, are already studied in chapter 5.

The hydrostatic stress field of the relaxed $\Sigma9(2\bar{2}1)$ GB with superimposed atomic positions is shown in Fig. 5.7 in chapter 5. As expected for a large-angle symmetrical GB, regions of large stress variations are visible only in the immediate vicinity of the GB. As a consequence of the GB structure there are five nonequivalent slip planes for the $\{\bar{1}12\}$ slip system indicated by numbers of 1 to 5 in Fig. 5.7. The previous calculations in chapter 5 have shown that an edge dislocation is transmitted through the GB only when gliding on the plane number 1 while it is absorbed by the GB on the other four planes. In the present thesis the focus is on one specific case, in which the dislocation gliding on the plane number 5 is blocked by the GB and subsequently acts as a crack nucleation site.

After the incoming dislocation is absorbed by the GB, the stress field of the edge dislocation is superimposed on the local stress field of the GB as shown in Fig. 5.8 in the above chapter. There are clear regions of tensile and compressive stresses below and above the absorption site, respectively. Applied biaxial tensile loadings can then lead to the nucleation of a crack in the tensile region underneath the absorbed dislocation. Nearly biaxial loading induces crack nucleation directly from the absorbed dislocation, followed by crack propagation and the seperation of the GB. The required stress levels are extremely high and not far from the ultimate strength of the perfect boundary. The results for the applied stresses at which crack nucleation occurrs are displayed in Fig. 6.1. The stress σ_{xx} for crack nucleation increase as σ_{yy} is increased.

Reducing the applied stress in y (for σ_{yy}/σ_{xx} below about 2/3) leads to a completely different failure mode which is characterized by the emission of dislocations from the region underneath the absorbed dislocation and subsequent crack nucleation. The critical stresses for this entire sequence of events to occur decreases quite significantly with decreasing σ_{yy}/σ_{xx} as shown in Fig. 6.1.

Fig. 6.2 shows the atomic configuration after crack nucleation following the emission of six dislocations. The emitted dislocations have the $a/2[\bar{1}11]$ Burgers vectors in the left grain and the $a/2[11\bar{1}]$ Burgers vectors in the right grain. The emission of dislocations with a Burgers vector which is almost opposite to the absorbed dislocation seems at first counterintuitive. However, under pure tensile loading, the absorbed dislocation would
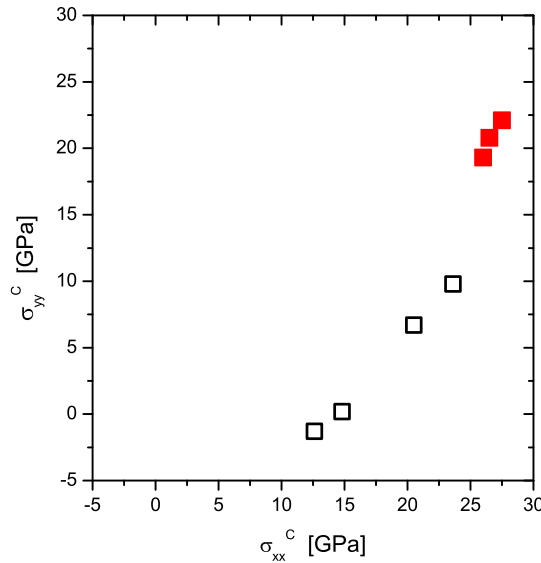
Figure 6.1: Critical stresses for crack nucleation at the $\Sigma 9(2\bar{2}1)$ GB in W under plane strain conditions in plane xy. The two regimes show crack nucleation without (filled points) or with prior (open points) dislocation emission.

experience a weak driving force out of the boundary. In contrast, the emitted dislocations, with the Burgers vectors of $a/2[1\bar{1}1]$ in the right grain and $a/2[\bar{1}11]$ in the left grain, glide on {211} planes inclined by 54.7° to the loading axis x and therefore experience nearly maximal driving forces. The dislocation emission occurs several atomic layers below the absorbed dislocation and only appears to be aided by the tensile stress field of the absorbed dislocation. The sites from which the dislocations are emitted correspond to regions of the GB with a large local tensile stress (see Fig. 5.7). A dislocation emission to the left grain is followed by a dislocation emission to the right grain four {211} planes blow corresponding to the periodicity of the GB in the $\langle 114 \rangle$ direction. Other four dislocations are emitted following the same sequence and totally six dislocations are emitted, three to the grain grain and three to the left grain. The tensile stress field of the six dislocations as well as the previously absorbed dislocation superimpose and the maximum value is found below the sixth dislocation. After the sixth dislocation is emitted into the right grain, a crack is nucleated below it.

Crack nucleation at the $\Sigma 9(\bar{1}14)$ GB is also simulated. The structure and the stress field of the GB can be found in Fig. 5.4(a) in chapter 5. An $a/2[1\bar{1}1]$ lattice dislocation coming on plane 1 is absorbed by the GB, as studied in chapter 5. The system is then relaxed without controlled boundary conditions, removing the applied shear strain. Biaxial tensile strain is applied to the relaxed system.

By applying uniaxial strain in x, twin emissions are found below the absorption site at the $\Sigma 9(\bar{1}14)$ GB. One twin is emitted into the right grain in the direction of $[1\bar{1}1]$, followed by the emission of the other twin into the left grain in the direction of $[\bar{1}1\bar{1}]$. As the twins grow into grain interiors, a crack is nucleated from the emission site (Fig. 6.3). When controlled top and bottom boundaries (numbered as 3 and 4 in Fig. 6.3) are freed
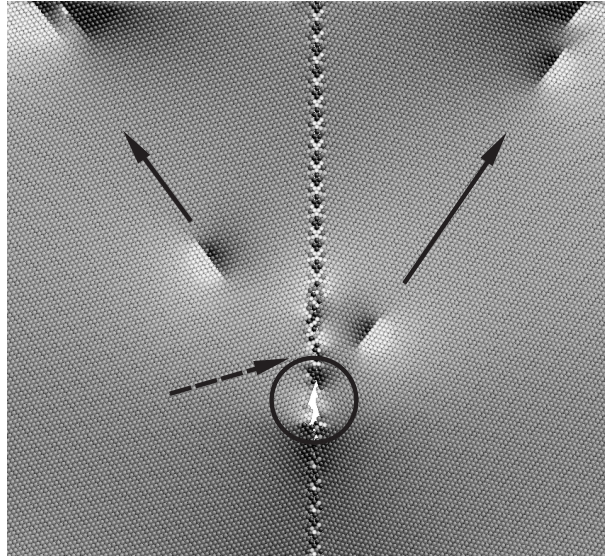
Figure 6.2: Crack nucleation at the $\Sigma 9(2\bar{2}1)$ GB in W under $\sigma_{yy} = 0$. Crack nucleation follows the absorption of one dislocation (indicated by the dashed arrow) and the emission of six edge dislocations (indicated by the solid arrows). Atoms are shaded by the hydrostatic stress. White shading represents compression and black represents tension.

which are corresponding to applied biaxial strain conditions, a twin is nucleated at the top surface of the right grain and grows in the direction of $[\bar{1}1\bar{1}]$ towards the $\Sigma 9(\bar{1}14)$ GB. A crack is nucleated at the GB after absorbing the growing twin (Fig. 6.4).

Different with the dislocation emissions at the $\Sigma 9(2\bar{2}1)$ GB before crack nucleation, twin emissions occur at the $\Sigma 9(\bar{1}14)$ GB. This is due to the twinning-antitwinning behavior. For the $\Sigma 9(2\bar{2}1)$ GB, dislocation emissions are favored by the applied stress state because the orientations of grains determine antitwinning directions in $[\bar{1}11]$ in the left grain and $[1\bar{1}1]$ in the right grain. However, for the $\Sigma 9(\bar{1}14)$ GB, twinning is favored in the directions where it is observed. The twin here can be viewed as a group of $a/6\langle 111\rangle$ edge dislocations superimposing each other in the direction of the twin width, with the number of layers of the twin width being the number of the dislocations. As can be seen in Fig. 6.3and Fig. 6.4, a strong stress field associated with a twin causes the crack nucleation at the $\Sigma 9(\bar{1}14)$ GB.
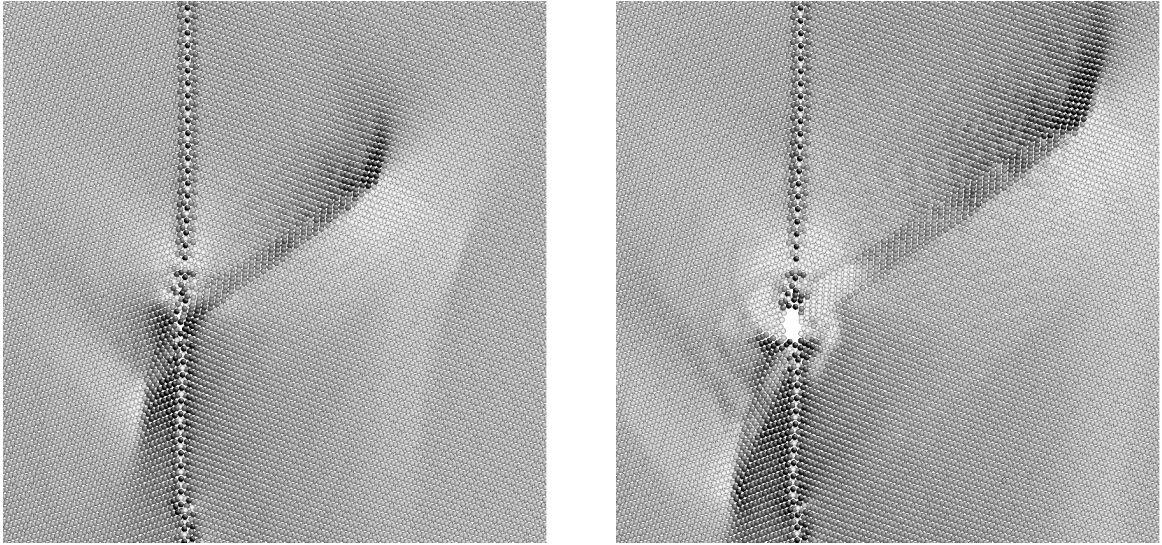
Figure 6.3: Crack nucleation at the $\Sigma 9(\bar{1}14)$ GB in W, following absorption of one $a/2[1\bar{1}1]$ edge dislocation coming from the left grain and emissions of two twins to the left and the right grains. Critical stresses for crack nucleation are $\sigma_{xx} = 21.5\ GPa$, $\sigma_{yy} = 11.2\ GPa$, $\sigma_{zz} = 9.8\ GPa$, and critical plane strains are $\epsilon_{xx} = 6.7\%$, $\epsilon_{yy} = 0$.
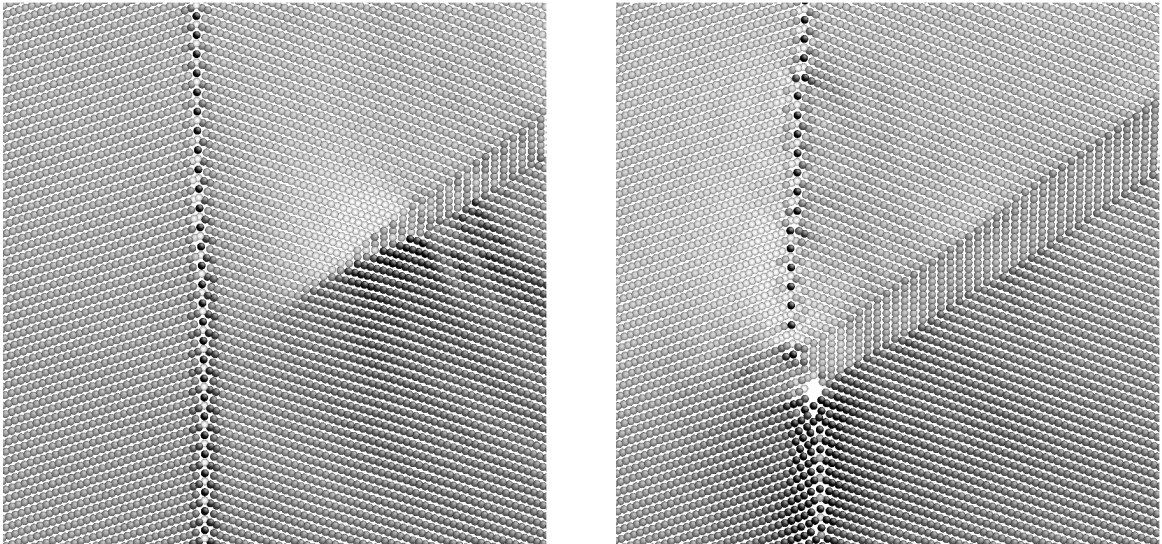

Figure 6.4: Crack nucleation at the $\Sigma 9(\bar{1}14)$ GB in W, following absorption of one growing twin from the top surface of the right grain. Critical stresses for crack nucleation are $\sigma_{xx} = 14.0\ GPa$, $\sigma_{yy} = 1.5\ GPa$, $\sigma_{zz} = 4.2\ GPa$, and critical plane strain conditions are $\epsilon_{xx} = 3.0\%$.

Chapter 7

Discussion, conclusion and outlook

7.1 Discussion

7.1.1 Small-angle tilt GBs

Comparing the two SAGBs in W with the same tilt axis: by varying the GB plane from (15 $\overline{15}$ 1) to (1$\overline{1}\overline{1}$), the GB energy decreases from 1.11 to 1.00 J/m^2 as predicted, even though the misorientation increased. The reason for this finding is related to the fact that the energy of SAGB is proportional to the GB dislocation density and the misorientation depends only on the Burgers vector content normal to the GB. The boundary in Fig. 3.2 includes dislocations whose Burgers vector is inclined to the GB plane and are therefore in literature also called wavy [16, 18]. Under these conditions the dislocation density and the GB energy are higher than those of the boundary shown in Fig. 3.5.

The GB shown in Fig. 3.2 is immobile under shear loadings. This is due to the self-locking of the GB dislocations, which glide a short distance on their inclined glide planes respectively till blocking. For this particular GB, the two types of GB dislocations move to the same side with respect to the GB but crossing is not possible at 0 K as the mutual interaction between them is repulsive and the motion due to the shearing leads to a local increase in the elastic energy. This high energy configuration cannot be overcome at low temperatures. This observation is independent of the shearing direction. A quite different behaviour is observed at tensile loadings normal to the GB plane. In this case the SAGB of 5.4° splits which is highly mobile as shown in Fig. 3.4. This simulation shows that the GB mobility depends strongly on both the GB dislocation content, the GB plane and the stress state acting on the GB. These findings show that there can be transitions from immobile to mobile GB behaviour as a function of the orientation of the GB plane relative to the constituent Burgers vectors and as a function of the applied stress state. The stress state that drives the GB motion is clearly not just the resolved shear stress on the geometrically necessary Burgers vector content according to the dislocation model. In contrast GB motion shows very clear non-Schmid behaviour from the geometrical point of view. Similar GB splitting are also simulated in Cu where the grouped glide motion of Shockley partial dislocations is thought as the mechanism and GB splitting is an interesting example of the GB controlled plasticity in nanocrystal materials [65].

The GB energy is higher for partial dislocations constructing the boundary based on our simulations because the dislocation density is higher compared to perfect constituent

dislocations. By comparing the two boundaries in aluminum, the tilt axis is clearly shown as a determining parameter of a boundary in boundary energies and mechanical properties, e.g. the energy of the GB in Fig. 3.6 is approximately equal to that in Fig. 3.7, though the tilt angle is about twice. Furthermore, they have different mobilities under shear loadings as describe in the following.

In the case of the [110] tilt SAGBs in Al, the GB dislocation structure shown in Fig. 3.6 is composed of three sets of dislocations, sessile Lomer dislocations and glissile 60° dislocations. The Lomer dislocation, can be constructed from lattice dislocations of the two grains. The glissile 60° dislocation is attracted by the neighbouring Lomer dislocations, which also stabilize the 60° dislocation under shear loadings. The [110] tilt SAGB are therefore immobile. The higher energy version of the [110] tilt boundary, with the supplementary 60° dislocation is found during the relaxation procedure described in chapter 2. Note that two of the 60° Burgers vectors can merge into one edge dislocation as $1/2[1\bar{1}0] = 1/2[10\bar{1}] + 1/2[0\bar{1}1]$, decreasing the GB energy and compensating the local twist by the paired dislocations. At first glance, the occurrence of the high energy version might be considered as an artificial outcome of the simulation, but a similar GB has been observed experimentally in Al [16]. In their interpretation [16], the compensation of a local twist component between the two grains has been raised as the reason for the occurrence of these inclined dislocations. Based on present simulation results, I conclude that this is not a necessary condition as the simulated GBs are of pure tilt type and can be regarded as a relatively stable interface of higher energy. For complex GB dislocations structures as in [16, 18], it is impossible to predict them by a simple geometry based theory, but atomistic simulations can produce several metastable states.

In the second studied [1$\bar{1}$2] tilt GB in Al, the influence of the tilt axis on the mobility can be seen: the constituent dislocations are glissile for both realization, either for perfect GB dislocation or for partial GB dislocations. These two types of GB dislocations have been found as the most frequently occurring outcomes. This shows that the systematic relaxation procedure is of most importance to find the perfect and the partial constituent dislocations in [1$\bar{1}$2] tilt boundary in Al. It is also interesting to study further Ni or Cu having lower stacking fault energies.

7.1.2 Dislocation interaction with GBs

Depending on the structure of the $\Sigma21(241)[1\bar{1}2]$ GB in Al and available slip systems in the neighboring grains, dislocation transmission is expected according to the geometrical criteria [23, 24] (the intersection angle between the incoming and the outgoing slip planes is zero; the magnitude of the Burgers vector left at the GB after dislocation transmission is small; the resolved shear stress on the outgoing dislocation is big). However, the interaction with only one incoming dislocation depends on the atomistic structure of the GB and the outcome can not be predicted by geometrical criteria. One single lattice dislocation coming on different glide planes ending at different sites in the GB is always absorbed by the GB, though the details of the absorption process differ. Different atomic configurations inside the core of the GB lead to different atomic stress states. The dislocation absorptions can be explained by the interaction between the stress fields of the dislocation core and the GB. The absorption process at the symmetrical tilt GB is always accompanied with the creation of GB dislocations, which can glide in the GB plane away

from the absorption site and cause GB migration.

Local stress concentration devolops at the $\Sigma21(241)[1\bar{1}2]$ symmetrical and the asymmetrical tilt GBs in Al when there are dislocation pile-ups from one grain. Dislocation emissions into the other grain can be enforced by the pile-ups containing a few dislocations. Resistance strengh against dislocation pile-ups vary at different sites in the symmetrical GB. Different with the symmetrical GB, the Burgers vector left at the GB after dislcoation transmission through the asymmetrical GB is not in the GB plane and thus the motion of the created GB dislocation is not favored at low temperatures. For dislocation transmission through the two large-angle GBs, the transmitted dislocations are generally qualified by all the conditions of previous criteria [23, 24].

Among the twelve major fcc slip systems for the case of the symmetrical $\Sigma21$ GB in Al, angles between the intersection lines of the incoming and the four outgoing slip planes with the symmetrical $\Sigma21$ GB are: $\beta(\bar{1}11)$ $0°$; $\delta(111)$ $37.37°$, $\alpha(1\bar{1}1)$ $71.86°$; $\gamma(11\bar{1})$ $90°$.

The simulated outgoing slip system has the Burgers vector of $a/2[110]^2$ and the slip plane of $\beta(\bar{1}11)^2$ (superscript ^{2} represents the right grain). The intersection angle is the lowest, $0°$, among the four slip planes. The magnitude of the residual Burgers vector $a/7[\bar{1}32]^2$ is small, $0.53a$, which is glissile in the GB plane.

Another candidate slip system is the one with the the Burgers vector of $a/2[10\bar{1}]^2$ and the slip plane of $\delta(111)^2$. Suppose this slip system is activated, the magnitude of the residual Burgers vector $a/14[\bar{2}1\bar{3}]^2$ is the minimum, $0.27a$. However, the creation of such a dislocation at the GB does not help to release the local stress concentration because it is not in the GB plane and the motion is restricted at low temperatures which requires atom shuffling. Furthermore, the outgoing slip plane is not favored because it is not co-planar with the incoming slip plane but has an intersection angle of $37.37°$. According to the criterion of [24], the magnitude of the residual Burgers vector left at the GB for this slip system is half of that for the observed outgoing slip system, this slip system is prefered to be activated, but not observed in the simulation. It means that the change of the slip planes is also a key factor and it is not easy to determine which one is of overriding importance. Previous criteria for dislocation transmission through GBs[23, 24] select the outgoing slip system with a minimum change of the Burgers vectors and slip planes. The change of slip planes may be more difficult than the change of Burgers vectors for most observations found only a small angle between the slip planes [23, 24]. The stronger dependence of the change of slip planes is also shown in our simulations here.

In the dislocation pile-ups at the asymmetrical large-angle GB from one grain, there are two interesting slip systems in the other grain for the emission of dislocations.

Angles between the intersection lines of the incoming and the four outgoing slip planes with the asymmetrical GB are: $\beta(\bar{1}11)$ $0°$; $\gamma(11\bar{1})$ $28.30°$; $\delta(111)$ $33.95°$; $\alpha(1\bar{1}1)$ $84.70°$.

A slip with the Burgers vector of $a/2[0\bar{1}\bar{1}]^2$ on plane $\gamma(11\bar{1})^2$ is activated in the neighboring grain with a small intersection angle, $28.30°$, among the four fcc outgoing slip systems, but not the one with the Burgers vector of $a/2[\bar{1}\bar{1}0]^2$ on plane $\beta(\bar{1}11)^2$ which is co-planar with the incoming slip plane. To compare the two slip systems, the dominant term is the angle between the incoming and outgoing Burgers vectors, which are $23.20°$ for the case of $a/2[0\bar{1}\bar{1}]^2$ and $74.77°$ for the case of $a/2[\bar{1}\bar{1}0]^2$, with residual Burgers vectors are $a/\sqrt{116}[2\sqrt{2}, \sqrt{29}-4\sqrt{2}, \sqrt{29}-3\sqrt{2}]^2$ and $a/\sqrt{116}[\sqrt{29}+2\sqrt{2}, \sqrt{29}-4\sqrt{2}, -3\sqrt{2}]^2$, respectively. The magnitude of the former is $0.28a$, wich is much smaller than the latter,

$0.86a$. The residual Burgers vectors both are not in the GB plane and the motion is restricted at low temperatures.

Though there is no quantitative determination whether there is dislocation transmission, the angle χ between the normal of the incoming slip plane and the normal of the GB plane should be a dominate parameter. When the angle is small, the stress from dislocation pile-ups provides locally a shear stress along the GB plane and therefore atoms rearrange more inside than perpendicular to the GB plane and transmission becomes more difficult. Dislocation absorption at the $\Sigma 9(\bar{1}14)$ GB in W is found in when χ is small, 54.74°, while dislocation transmissions through two other GBs are found when χ are big, 70.53° and 74.21°. In present simulations of dislocation pile-ups at the two large-angle GBs in Al, the angles of χ are both big, 67.79° for the symmetrical GB and 90° for the asymmetrical GB, transmissions are efficient and found in the simulation. When χ is small, 58.52°, a few dislocations can be absorbed at the coherent $\Sigma 11$ GB in Al and cause highly damage at the absorption site [38]. Regardless of which outgoing slip system is activated, the transmission may be a function of χ.

From the simulations of the dislocation interaction with three representative tilt GBs in Al, it is found that the capacity of atomicly the same site in GBs for absorbing dislocations is one. GBs may absorb more dislocations through GB plasticities if there are no efficient slip systems activated in neighboring grains. Though criteria for dislocation transmissions work well with the simulation results, criteria should be regarded as necessary, not sufficient, conditions since the details of dislocation transmissions are affected by many factors which are still poorly known. The complexity of dislocation-GB interactions is shown in Fig. 2.1. The outcome of their interactions can not be easily captured by dislocation transmission criteria [23, 24, 33], as shown by the atomistic simulations, because it depends on the sign of the incoming lattice dislocations (cross symbol in Fig. 2.1), the interacting sites at GBs (1 or 2), the size of dislocation pile-ups (the number of dislocations in the pile-up), the GB structure, the available slip systems in neighboring grains (co-planar or non-co-planar, or the angles between the incoming and outgoing slip planes) and the applied loadings.

The simulation results of dislocation-GB interactions in W show that the GB structure itself is a key factor for dislocation absorption or transmission. Another key factor is the angle between the incoming Burgers vector and the axis of the GB.

Comparing to the stress concentration inside a dislocation core, the local stress level of the coherent $\Sigma 3$ GB is very low which can be viewed as there are no stress barriers for the incoming dislocation. Furthermore, the angle between the two slip planes in either grains is small. Therefore dislocation transmission is found. For the other two incoherent $\Sigma 9$ boundaries, grain boundary atoms are in a high stress level as that of a dislocation core and provide considerable attractive or repulsive forces to coming dislocations. The compressive part of the dislocation core neutralizes the local tensile stresses in the GB and vice versa. This can eventually lead to significant rearrangements in the boundary plane and to the immediate absorption of the dislocation and creations of disconnections. On the other hand, when there is a high angle between the two neighboring slip planes ($\Sigma 9(\bar{1}14)$), an incoming dislocation is absorbed because of the atom rearrangement in the direction of GB plane.

The defect at the absorption site is called a disconnection in concept of [61] or a ledge

in other papers [66]. A disconnection consists a GB step and a GB dislocation. Atom arrangement around the absorption site is much disordered. The GB step is not a pure step but inherits the stress field of the core of the absorbed lattice dislocation. The GB dislocation induced GB migration [67, 68] may restore the original GB structure [61] or not depending on the migration direction with the step direction. The motion of the GB dislocation in the GB plane increases the GB step as in the $\Sigma 9(\bar{1}14)$ GB. While in the $\Sigma 3$ and the $\Sigma 9(2\bar{2}1)$ GBs, the original GB structure is restored by the GB migration. GB migration in conjunction with the dislocation transmission appears to be a frequently observed phenomenon (see aslo [36, 66]). The GB dislocations are supposed to facilitate GB migration [61]. In all three cases, GB migration occurs at an obvious lower strain involving GB dislocations. The critical shear strains for the migration of pure GBs are 1.6%, 3.2% and 2.5% respectively. Note that the GB dislocation may not propagate when the applied shear strain is small even it is glissile in the plane. Otherwise, it is hard to move as in asymmetrical boundaries or the local atom arrangement is disordered. The GB dislocation stays near the absorption site and makes the local structure more disordered. Further dislocation pile-ups may increase the step and make a boundary kink band as usually observed.

Based on our results, dislocation transmission through a GB in general is more complicated than previously assumed. Even in the seemingly ideal cases studied here, where glide planes meet on a common line in the plane of the boundary and where the residual Burgers vector at the GB after dislocation transmission is small, is the transmission of the dislocation through the $\Sigma 9(2\bar{2}1)$ GB in W a rare event. Dislocation absorption and spreading of the dislocation core along the boundary - introducing climb dissociation in the plane of the boundary - is more frequent. Consequently, purely kinematic, stress based transmission criteria appear to be applicable only to very special cases like coherent GBs [36, 1]. In a more general setting, the transmission should probably rather be viewed as a thermally activated re-nucleation event as proposed in [33]. Whether it is sufficient to just focus on the residual Burgers vector as a measure of the activation energy (as in [33]) is, however, again questionable. The criteria for dislocation transmission based on microscopic observations [23, 24], which considers mainly the geometrical relationship between the two slip systems in neighboring grains and no atomic processes, are only necessary conditions.

7.1.3 Crack nucleation

The dislocation emission at the $\Sigma 9(2\bar{2}1)$ GB in W effectively deposits dislocations with the opposite Burgers vector into the GB. These are stacked so as to effectively produce a wedge disclination dipole, which is separated further as additional dislocations are emitted (Fig. 7.1). Thereby the tensile stress field underneath the deposited dislocations increases and extends over longer distances, which then eventually leads to crack nucleation. In this sense the final crack nucleation event can be analyzed in a similar spirit as the intersection of twins of different height [42]. Crack nucleation from twin absorption or emission are simulated and the critical strain is decreased significantly comparing to the separation of the pure GB.

Since the dislocation emission at the $\Sigma 9(2\bar{2}1)$ GB or the twin emission at the $\Sigma 9(\bar{1}14)$ GB prior to crack nucleation appears to be the critical step in this mechanism it is
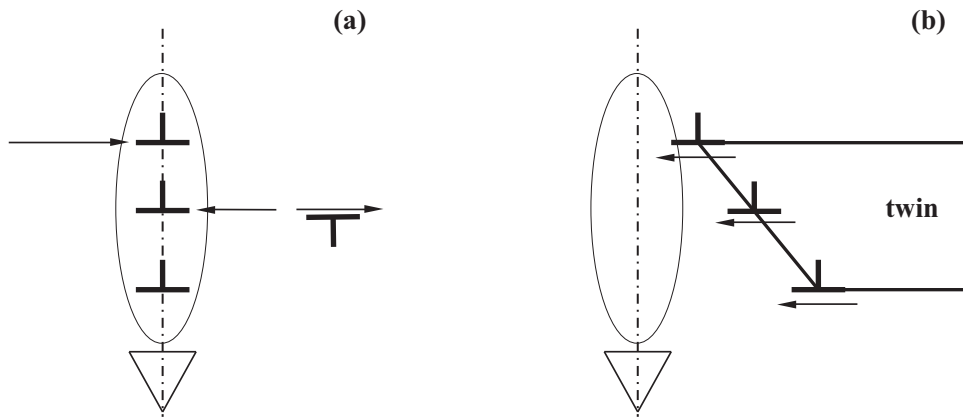
Figure 7.1: Schematic drawing of the mechanisms of crack nucleation from absorption/emission of dislocations (a) or twins (b).

not surprising to find that the critical stresses decrease as the biaxiality decreases and, consequently, the resolved shear stresses on the glide planes increase. The simulation clearly shows that the crack nucleation is a complex process which depends sensitively on other applied stresses as well as GB structure and cannot be fully explained by simple pile-up nucleation models. In this sense, the mechanism proposed here can be explained as a disclination model or dislocation pile-ups at GB planes, which is a complement to the pile-up model that can be regarded as dislocation pile-ups perpendicular to the GB plane.

7.2   Conclusion

By atomistic simulations, the energies and mobilities of SAGBs are shown to be determined by the characteristics of constituent GB dislocations. For SAGBs with one macroscopic description in terms of the 5 free order parameters to describe a GB completely, several possible GB dislocation arrangements have been found with different GB energies. Selected examples show the predictions that the mobility of SAGBs depends on the sessile or glissile characteristics of constituent dislocations, the number of types and arrangements of them which determine the local interaction between them, and the external loadings which is shown to make a GB immobile under shear but splitting under tension along the normal of the GB plane. The dislocation arrangement and the mobility of SAGBs is also important for the interaction of incoming dislocations with preexisting SAGBs.

The atomistic process of the interactions between edge dislocations and three representative $[1\bar{1}2]$ tilt GBs in fcc aluminum is studied. The interaction between dislocation cores determines the outcome of dislocation-GB interactions because small-angle GBs are constructed by isolated dislocations. One incoming lattice dislocation is always absorbed by the two studied large-angle GBs, the symmetrical $\Sigma 21$ and the asymmetrical large-angle $[1\bar{1}2]$ tilt GBs. The absorption is controlled by atomistic mechanisms and can not be predicted by geometrical dislocation transmission criteria. Dislocation pile-ups at the two large-angle GBs are simulated and different behavior of dislocation absorption and

transmission is found for the symmetrical GB by varying the interacting sites at the GBs and the size of the dislocation pile-ups, which means that different sites in the GB can give different resistance strength to dislocation pile-ups. Dislocation emission into one grain is also found from the asymmetrical large-angle GB when two dislocations pile up at the GB from the other grain in the bicrystal. The transmitted slip systems through the two large-angle GBs always have minimum changes with the incoming slip systems both in the Burgers vectors and the slip planes, generally fulfill geometrically all the conditions in previous criteria. The angle between the normal of the incoming slip plane and the normal of the GB plane is pointed out to be also a dominate parameter controlling the outcome of dislocation-GB interactions.

Dislocation-GB interaction in tungsten studied by atomistic simulations shows that the dislocation may be absorbed, stopped in front of the boundary or transmitted, depending on the GB structure, the slip systems in neighboring grains and sensitively on the impacting sites. This can be explained by the interaction of the stress field of the dislocation core with the local stress field of the GB. Furthermore, GB migration is found to accompany the transmission process in these symmetrical tilt GBs.

Crack nucleation at the $\Sigma 9(2\bar{2}1)$ and the $\Sigma 9(\bar{1}14)$ tilt GBs is simulated in tungsten from an absorbed dislocation. A crack is nucleated at the $\Sigma 9(2\bar{2}1)$ GB just underneath the absorption site under nearly biaxial loading conditions. However, more uniaxial loading causes failure to occur at lower stresses and the crack nucleation follows the emission of several dislocations. Crack nucleations at the $\Sigma 9(\bar{1}14)$ tilt GBs follows the emission of twins into grain interior or the absorption of a growing twin. Our study shows that the process of crack nucleation at the atomic level is thus more complex than previously anticipated.

7.3   Limitation and outlook

The study in this thesis is restricted to tilt GBs and edge dislocations. The interactions between screw dislocations or mixed dislocations and GBs are demanded for a general understanding. More large scale 3D atomistic simulations are needed to study general interactions between dislocations and GBs. Quantitative criteria for dislocation-GB interactions are very important as input to mesoscale simulations, which can be proposed and tested by atomistic simulations. Crack nucleation at other GBs in W involving dislocation activities using more accurate interatomic potentials are needed to understand the mechanism. At higher temperatures, GB diffusions become more active which is coupled with GB migration and sliding (e.g. Coble creep [69]). A competition between GB plasticity and dislocation activities is expected to carry the dominant plastic deformations, especially in nanocrystals and thin films [70]. This is still unknown and more experiments [71] and simulations are needed to uncover it.

Bibliography

[1] J.P. Hirth and J. Lothe. *Theory of dislocations*. Krieger Publishing Company, Florida, 1982.

[2] J. Schiøtz, T. Vegge, F.D. Di Tolla, and K.W. Jacobsen. *Phys. Rev. B*, 60:11971, 1999.

[3] J.D. Rittner and D.N. Seidman. *Phys. Rev. B*, 54:6999, 1996.

[4] R. Phillips. *Crystals, Defects and Microstructures*. Cambridge University Press, 2001.

[5] S. Suresh. *Fatigue of Materials*. Cambridge University Press, 1991.

[6] A.P. Sutton. *International Metals Reviews*, 29:377, 1984.

[7] A.P. Sutton and R.W. Balluffi. *The theory of transformations in metals and alloys*. Oxford University Press, New York, 1996.

[8] G.I. Taylor. *Proc. Roy. Soc. London A*, 145:388, 1934.

[9] J.M. Burgers. *Proc. Phys. Soc. (London)*, 52:23, 1940.

[10] W.T. Read and W. Shockley. *Phys. Rev.*, 78:275, 1950.

[11] Z. Zhang, W. Sigle, and M. Ruehle. *Phys. Rev. B*, 66:094108, 2002.

[12] R.A. De Souza, J. Fleig, J. Maier, O. Kienzle, Z. Zhang, W. Sigle, and M. Ruhle. *J. Am. Ceram. Soc.*, 86:922, 2003.

[13] Z. Zhang, S. Wilfried, R.A. De Souza, K. Wolfgang, M. Joachim, and R. Manfred. *Acta Mater.*, 53:5007, 2005.

[14] N.F. Mott. *Proc. Phys. Soc. (London)*, 60:391, 1948.

[15] M. Winning and A.D. Rollett. *Acta Mater.*, 53:2901, 2005.

[16] J.M. Penisson and A. Bourret. *Phil. Mag. A*, 40:811, 1979.

[17] A. Bourret and J. Desseaux. *Phil. Mag. A*, 39:405, 1979.

[18] C.L. Johnson, M.J. Hÿtch, and P.R. Buseck. *PNAS*, 101:17936, 2004.

[19] M.F. Chisholm and D.A. Smith. *Phil. Mag. A*, 59:181, 1989.

[20] H. Van Swygenhoven, D. Farkas, and A. Caro. *Phys. Rev. B*, 62:831, 2000.

[21] U. Wolf, P. Gumbsch, H. Ichinose, and H.F. Fischmeister. *Colloque de Physique*, 51:C1–359, 1990.

[22] E. Ernst, M.W. Finnis, D. Hofmann, T. Muschik, U. Schönberger, U. Wolf, and M. Methfessel. *Phys. Rev. Lett.*, 69:620, 1992.

[23] Z. Shen, R.H. Wagoner, and W.A.T. Clark. *Acta Metall.*, 36:3231, 1988.

[24] T.C. Lee, I.M. Robertson, and H.K. Birnbaum. *Phil. Mag. A*, 62:131, 1990.

[25] B. Chalmers. *Proc. R. Soc. London A*, 162:120, 1937.

[26] C. Zener. *Fracturing of Metals*, American Society for Metals:3, 1948.

[27] N.J. Petch. *J. Iron Steel Institute*, 11:22, 1953.

[28] T.L. Johnston, R.J. Stokes, and C.H. Li. *Phil. Mag.*, 7:23, 1962.

[29] B.J. Pestman, J.T.M. De Hosson, V. Vitek, and F.W. Schapink. *Phil. Mag. A*, 64:951, 1991.

[30] M. de Koning, R. Miller, V.V. Bulatov, and F.F. Abraham. *Phil. Mag. A*, 82:2511, 2002.

[31] T. Zhu, J. Li, A. Samanta, H.G. Kim, and S. Suresh. *PNAS*, 104:3031, 2007.

[32] Y. Cheng, M. Mrovec, and P. Gumbsch. *Mater. Sci. Eng. A*, xx:xx, 2007.

[33] A. Ma, F. Roters, and D. Raabe. *Acta Mater.*, 54:2181, 2006.

[34] J.D. Livingston and B. Chalmers. *Acta Metall.*, 5:322, 1957.

[35] V. Yamakov, D. Wolf, S.R. Phillpot, A.K. Mukherjee, and H. Gleiter. *Nature Materials*, 1:45, 2002.

[36] Z. Jin, P. Gumbsch, E. Ma, K. Albe, K. Lu, H. Hahn, and H. Gleiter. *Scripta Mater.*, 54:1163, 2006.

[37] V.B. Shenoy, R. Miller, E.B. Tadmor, R. Phillips, and M. Ortiz. *Phys. Rev. Lett.*, 80:742, 1998.

[38] M. Dewald and W.A. Curtin. *Modelling Simul. Mater. Sci. Eng.*, 15:S193, 2005.

[39] C. Brandl, E. Bitzek, P.M. Derlet, and H. Van Swygenhoven. *Appl. Phys. Lett.*, 91:111914, 2007.

[40] M. Polcarova, J. Gemperlova, J. Bradler, A. Jacques, and A. George andPhil. Mag. A L. Priester. *Phil. Mag. A*, 78:105, 1998.

[41] A. Gemperle, J. Gemperlova, and N. Zarubova. *Mat. Sci. Eng. A*, 387-389:46, 2004.

[42] P. Müllner, C. Solenthaler, and P. J. Uggowitzer. *Acta Metall. Mater.*, 42:2211, 1994.

[43] G. Subhash, Y.J. Lee, and G. Ravichandran. *Acta Metall. Mater.*, 42:319, 1993.

[44] W.S. Lee, C.F. Lin, and G.L. Xiea. *Mat. Sci. Eng. A*, 247:102, 1998.

[45] T. Dummer, J. Lasalvia, G. Ravichandran, and M. Meyers. *Acta Mater.*, 46:6267, 1998.

[46] R. Margevicius, J. Riedle, and P. Gumbsch. *Mat. Sci. Eng. A*, 270:197, 1999.

[47] http://www.itap.physik.uni stuttgart.de/∼imd/.

[48] M.W. Finnis and J.E. Sinclair. *Phil. Mag. A*, 50:45, 1984.

[49] G.J. Ackland and R. Thetford. *Phil. Mag. A*, 56:15, 1987.

[50] Y. Mishin, D. Farkas, M.J. Mehl, and D.A. Papaconstantopoulos. *Phys. Rev. B*, 59:3393, 1999.

[51] F. Ercolessi. *A molecular dynamics primer*. Spring College in Computational Physics, ICTP, Trieste, Italy, 1997.

[52] E. Bitzek, P. Koskinen, F. Gähler, M. Moseler, and P. Gumbsch. *Phys. Rev. Lett.*, 97:170201, 2006.

[53] W.H. Press, S.A. Teukolsky, W.T. Vetterling, and B.P. Flannery. *Numerical Recipes in C: The Art of Scientific Computing*. Cambridge Unviersity Press, 1992.

[54] http://www.gnuplot.info.

[55] J. Li. *Model. Simul. Mater. Sci. Eng.*, 11:173, 2003.

[56] J.D. Honeycutt and H.C. Andersen. *J. Phys. Chem.*, 91:4950, 1987.

[57] M. Born and K. Huang. *Dynamical Theory of Crystal Lattices*. Clarendon Press, 1954.

[58] M.J. Buehler, A. Hartmaier, H. Gao, M. Duchaineau, and F.F. Abraham. *Comput. Methods Appl. Mech. Eng.*, 193:5257, 2004.

[59] J.A. Zimmerman, E.B. Webb III, J.J. Hoyt, R.E. Jones, P.A. Klein, and D.J. Bammann. *Modelling Simul. Mater. Sci. Eng.*, 12:S319, 2004.

[60] A.F. Wright and S.R. Atlas. *Phys. Rev. B*, 50:15248, 1994.

[61] J.P. Hirth, R.C. Pond, and J. Lothe. *Acta Mater.*, 54:4237, 2006.

[62] M. Yamaguchi and V. Vitek. *J. Phys. F: Metal Phys.*, 5:1, 1975.

[63] M. Yamaguchi and V. Vitek. *J. Phys. F: Metal Phys.*, 5:11, 1975.

[64] J.W. Christian. In *Proc. 3rd Int. Conf. on Reinstoffe in Wissenschaft und Technik*, page 263. Akademie-Verlag., Berlin, 1970.

[65] J. Schiøtz, T. Rasmussen, K.W. Jacobsen, and O.H. Nielsen. *Phil. Mag. Lett.*, 74:339, 1996.

[66] D.E. Spearot, K.I. Jacob, and D.L. McDowell. *Acta Mater.*, 53:3579, 2005.

[67] C. Molteni, N. Marzari, M.C. Payne, and V. Heine. *Phys. Rev. Lett.*, 79:869, 1997.

[68] N. Chandra and P. Dang. *J. Mater. Sci.*, 34:656, 1998.

[69] R.L. Coble. *J. Appl. Phys.*, 34:1679, 1963.

[70] Y. Wei and H. Gao. Mater. Sci. Eng. A, in press.

[71] J. Rajagopalan, J.H. Han, and M.T.A. Saif. *Science*, 315:1831, 2007.

Acknowledgements

Resume

Name   Yuanfeng Cheng
E-mail   cheng@izbs.uni-karlsruhe.de, yuanfeng_cheng@yahoo.com.cn
Birthday   December 06, 1978
Homeplace   Jinxiang, Shandong Province, P.R. China

EDUCATION
08/2004-11/2007 PhD candidate, Mech Engr, University of Karlsruhe, Germany
02/2003-07/2004 Visiting Student, Geodynamics, Weizmann Institute of Science, Israel
1999-2002 M.S., Engr Mechanics, Tsinghua University, China, (Grade: 5th/30)
1995-1999 B.S., Engr Mechanics, Dalian University of Technology, China, (Grade: 2nd/40)

PUBLICATION
Cheng YF, Yang DH, Yang HZ, Biot/squirt model in viscoelastic porous media, 2002 Chin. Phys. Lett., 19, 445
Cheng Y, Mrovec M, Gumbsch P, Crack nucleation at the $\Sigma 9(2\bar{2}1)$ symmetrical tilt grain boundary in tungsten, 2007 Mater. Sci. Eng A, in press
Cheng Y, Mrovec M, Gumbsch P, Dislocation interaction with the local stress field of symmetrical tilt grain boundaries in body centred cubic tungsten, accepted to Phil. Mag.

LANGUAGE
English: TOEFL 593 (Test of Written English 5.0/6.0), GRE 2160

AWARDS
School's Excellent Student Scholarship, Dalian University of Tech., 1995-1998

TEACHING & RESEARCH ASSISTANT EXPERIENCE
Research Assistant, Weizmann Institute of Science, 02/2003-07/2004
Teaching Assistant, Tsinghua University, 01/2000-07/2001